Data assimilation for continuous global assessment of severe conditions over terrestrial surfaces

Clément Albergel[1], Yongjun Zheng[1], Bertrand Bonan[1], Emanuel Dutra[2], Nemesio Rodríguez-Fernández[3], Simon Munier[1], Clara Draper[4], Patricia de Rosnay[5], Joaquin Muñoz-Sabater[5], Gianpaolo Balsamo[5], David Fairbairn[5], Catherine Meurey[1], Jean-Christophe Calvet[1]

[1] CNRM, Université de Toulouse, Météo-France, CNRS, Toulouse, France

[2] Instituto Dom Luiz, IDL, Faculty of Sciences, University of Lisbon, Portugal

[3] CESBIO, Université de Toulouse, CNRS, CNES, IRD, Toulouse, France

[4] CIRES/NOAA Earth System Research Laboratory, Boulder, CO, USA

[5] European Centre for Medium-Range Weather Forecasts, Shinfield Road, Reading RG2 9AX, UK

*** Correspondence: clement.albergel@meteo.fr**

Abstract-This study demonstrates that LDAS-Monde, a global and offline Land Data Assimilation System (LDAS), that integrates satellite Earth Observations into the ISBA (Interaction between Soil Biosphere and Atmosphere) Land Surface Model (LSM), is able to detect, monitor and forecast the impact of extreme weather on land surface states. LDAS-Monde jointly assimilates satellite derived Earth observations of Surface Soil Moisture (SSM) and Leaf Area Index (LAI). First, LDAS-Monde is run at a global scale forced by the latest atmospheric reanalysis from the European Centre for Medium Range Weather Forecast (ECMWF), ERA5 (ECMWF fifth global reanalysis, LDAS_ERA5 hereafter) over 2010-2018, leading to a 9-yr, ~0.25° x 0.25° spatial resolution reanalysis of Land Surface Variables (LSVs). The quality of this global analysis is evaluated using several satellite-based datasets: assimilated SSM and LAI, but also independent datasets of evapotranspiration, Gross Primary Production, Sun Induced Fluorescence and snow cover. In addition, in situ measurements of SSM, evapotranspiration and river discharge are also employed for the evaluation. This assessment is conducted by comparing LDAS-Monde analysis with a model simulation (open-loop, no assimilation). Secondly, the global analysis is used to (i) detect regions exposed to extreme weather such as droughts and heatwave events and (ii) address specific monitoring and forecasting requirements of LSVs for those regions. This is performed by computing anomalies of the land surface states. They display strong negative values for LAI and SSM in 2018 for two regions experiencing severe heatwave and/or droughts: North Western Europe and the Murray-Darling basin in South Eastern Australia. For those two regions, monitoring and forecasting LSVs under extreme conditions are examined by forcing LDAS-Monde with ECMWF Integrated Forecasting System (IFS) high resolution operational analysis (LDAS_HRES, ~0.10° x 0.10° spatial resolution) over 2017-2018. Monitoring capacities are studied by comparing open-loop

and analysis experiments again against the assimilated observations. Forecasting abilities are assessed by initializing 4- and 8-day LDAS_HRES forecasts of the LSVs with the LDAS_HRES assimilation run compared to open-loop experiments. The impact of initialization in forecast mode is particularly visible for LAI that evolves at a slower pace than SSM and is more sensitive to initial conditions than to atmospheric forcing, even at an 8-day lead time. This highlights the importance of initial conditions to forecast LSVs and it confirms that LDASs should jointly analyse both soil moisture and vegetation states.

1 Introduction

Extreme weather and climate events like heatwaves and droughts are likely to increase in frequency and/or magnitude (IPCC, 2012, Ionita et al., 2017). Amongst all the natural disasters, droughts are the most detrimental (Bruce, 1994; Obasi, 1994; Cook et al., 2007; Mishra and Singh, 2010; WMO 2017) and about one-fifth of damages caused by natural hazards can be attributed to droughts (Wilhite 2000). They also cost society billions of dollars every year (WMO, 2017). It is therefore of paramount importance to implement tools that can monitor and warn about drought conditions (Svoboda, 2002; Luo and Wood, 2007; Blyverket et al., 2019) as well as their impact on land surface variables (LSVs) and society (Di Napoli et al., 2019). A major scientific challenge in relation to the adaptation to climate change is to observe and simulate how land biophysical variables respond to those extreme events (IPCC, 2012).

Droughts can be described as a deficit of water caused by a lack of precipitation. This definition is broad but droughts are generally classified according to the part of the hydrological cycle that suffers from a water deficit (IPCC, 2014; Barella-Ortiz and Quintana-Seguí, 2018). Drought types are all related to precipitation deficit and they have severe impacts in regions with rain-fed crops and no possible irrigation. They include meteorological droughts (lack of precipitation), agricultural droughts (deficit of water in the soil), hydrological droughts (deficit of streamflow, water level in rivers) and environmental droughts (a combination of the previous droughts types). Because of the effect of precipitation deficit on the whole hydrological system, all drought types are related (Wilhite, 2000). Complex interactions between continental surface and atmospheric processes have to be combined with human action in order to fully understand the wide ranging impacts of droughts on land surface conditions (Van Loon, 2015). As a consequence, Land Surface Models (LSMs) driven by high-quality gridded atmospheric variables and coupled to river-routing system are key tools to address these challenges (Dirmeyer et al., 2006; Schellekens et al., 2017). Initially developed to provide boundary conditions to atmospheric models, LSMs can now be used to monitor and forecast land surface conditions (Balsamo et al., 2015; Balsamo et al., 2018;

Schellekens et al., 2017). Additionally, the representation of LSVs by LSMs can be improved by coupling them with other models of the Earth system like atmosphere, oceans, river routing systems (e.g., de Rosnay et al., 2013, 2014; Kumar et al., 2018, Balsamo et al., 2018; Rodríguez-Fernández et al., 2019; Muñoz-Sabater et al., 2019).

Complementary to LSMs are Earth Observations (EOs). Satellite products are particularly relevant for the monitoring of LSVs. Satellite EOs related to the terrestrial hydrological, vegetation and energy cycles are now available at a global scale at kilometric scale and below and with long-term records (e.g., Lettenmaier et al., 2015, Balsamo et al., 2018). Combining EOs and LSMs through Land Data Assimilation Systems (LDASs) leads to enhanced initial land surface conditions (e.g. Reichle et al., 2007; Lahoz and De Lannoy, 2014; Kumar et al., 2018; Albergel et al., 2017, 2018a, 2019; Balsamo et al., 2018), which, in turn, lead to improved forecasts of weather patterns, sub-seasonal temperature and precipitation, agricultural and vegetation productivity, seasonal streamflow, floods and droughts, as well as the carbon cycle (Bamzai and Shukla, 1999; Schlosser and Dirmeyer, 2001; Bierkens, M. and van Beek, 2009; Koster et al., 2010; Bauer et al., 2015; Massari et al, 2018; Albergel et al., 2018a, 2019, Rodríguez-Fernández et al., 2019; Muñoz-Sabater et al., 2019). Amongst the current land-only LDAS activities several are NASA-led (National Aeronautics and Space Administration) projects. Examples of such activities are the Global Land Data Assimilation System (GLDAS, Rodell et al., 2004) which is run at a global scale. While the North American Land Data Assimilation System (NLDAS, Xia et al., 2012a, b) and the National Climate Assessment-Land Data Assimilation System (NCA-LDAS, Kumar et al., 2016, 2018, 2019) are run over the continental United States of America and the Famine Early Warning Systems Network (FEWS NET) Land Data Assimilation System (FLDAS, McNally et al., 2017) is run e.g. over Western, Eastern and Southern Africa. Finally, the Carbon Cycle Data Assimilation System (CCDAS, Kaminski et al., 2002), the Coupled Land Vegetation LDAS (CLVLDAS, Sawada and Koike, 2014, Sawada et al., 2015), the Data Assimilation System for Land Surface Models using CLM4.5 proposed by Fox et al., 2018, the SMAP (Soil Moisture Active Passive) level 4 system (Reichle et al., 2019) as well as LDAS-Monde (Albergel et al., 2017, 2018, 2019) developed by the research department of Météo-France are additional examples of data assimilation systems combining EOs and LSMs . Few studies have, however, included the assimilation of multiple EOs and considered global applications (Kumar et al., 2018, Albergel et al., 2019). A more detailed description of the various existing LDASs is available in Kumar et al., 2018, Albergel et al., 2019 and references therein.

After several applications at regional and continental scales (Albergel et al., 2017, 2018, 2019, Leroux et al., 2018, Tall et al., 2019, Blyverket et al., 2019, Bonan et al., 2020), LDAS-Monde is

run at a global scale forced by the latest atmospheric reanalysis from the European Centre for Medium Range Weather Forecast (ECMWF), ERA5, over 2010-2018 leading to a 9-yr, 0.25° x 0.25° spatial resolution reanalysis of the LSVs (LDAS_ERA5). In this paper, stemming from previous studies referenced above, it is shown that LDAS-Monde, by integrating jointly Surface Soil Moisture (SSM) and Leaf Area Index (LAI) EOs into the ISBA (Interaction between Soil Biosphere and Atmosphere) LSM (Noilhan and Planton, 1989, Noilhan and Mahfouf, 1996) at a global scale and in offline mode, can be used to detect, monitor and forecast the impact of extreme events on LSVs. The following items are presented and discussed in this study:

- An evaluation of LDAS-Monde at a global scale is carried out. This assessment involves the assimilated observations to demonstrate that the system is working as intended. But more fundamentally, LDAS-Monde global analysis is appraised using diverse, independent and complementary satellite-derived datasets of evapotranspiration (EVAP) from the GLEAM project (Miralles et al., 2011, Martens et al., 2017), Gross Primary Production (GPP) from the FLUXCOM project (Tramontana et al., 2016, Jung et al., 2017), Solar Induced Fluorescence (SIF) from the GOME-2 (Global Ozone Monitoring Experiment-2) scanning spectrometer (Munro et al., 2006, Joiner et al., 2016) and snow cover data from the Interactive Multi-sensor Snow and Ice Mapping System (or IMS, https://www.natice.noaa.gov/ims/, last accessed June 2019). This evaluation is additionally performed with in situ measurements of evapotranspiration from the FLUXNET 2015 synthesis data set (http://fluxnet.fluxdata.org/, last accessed June 2019), soil moisture from the International Soil Moisture Network (ISMN, https://ismn.geo.tuwien.ac.at/en/, last accessed June 2019) and river discharge from several networks across the world.
- LDAS-Monde global analysis over 2010-2018 is used to detect regions exposed to extreme weather such as droughts and heatwave events in 2018. This identification is performed by computing anomalies of LSVs over the 9-year period and identifying where strongest negative anomalies are located in 2018. For spotted regions, the monitoring and forecast abilities of LDAS-Monde are further investigatedat higher spatial resolution, thus exploring LDAS-Monde capacities to predict the evolution of LSVs in the context of droughts.

The paper is organised in five sections: section 2 details the various components constituting LDAS-Monde (the ISBA LSM, the data assimilation scheme and the EOs assimilated as well as the different atmospheric forcing datasets used), followed by the experimental and evaluation setup. Section 3 describes and discusses the impact of the analysis on the representation of the LSVs. Section 4 details the identification of 2 case studies over regions particularly affected by extreme events during 2018 and their detailed monitoring at higher spatial resolution combined with land

surface forecasting activities is also presented. Finally section 5 provides conclusions and prospects for future work.

2 Material and methods

The following subsections briefly describe the main components of LDAS-Monde: the ISBA LSM, its data assimilation scheme and two other key elements of the setup: atmospheric forcing and assimilated satellite derived observations. The experimental setup and the evaluation datasets used in this study are also presented.

2.1 LDAS-Monde

Embedded within the SURFEX (SURFace EXternalisée, Masson et al., 2013, version 8.1) modelling platform developed by the research department of Météo-France (CNRM, Centre National de Recherches Météorologiques), LDAS-Monde (Albergel et al., 2017) allows the joint integration of satellite derived SSM and LAI into the CO_2-responsive (Calvet, et al., 1998, 2004, Gibelin et al., 2006), multilayer diffusion scheme (Boone et al., 2000, Decharme et al., 2011) version of the ISBA LSM (Noilhan and Planton, 1989, Noilhan and Mahfouf, 1996) coupled with the CTRIP (CNRM Total Runoff Integrating Pathways, Decharme et al., 2019) hydrological model using a Simplified Extended Kalman Filter (SEKF, Mahfouf et al., 2009).

2.1.1 ISBA Land Surface Model

The ISBA LSM aims to model the evolution of LSVs. In the chosen configuration for this paper, ISBA is able to represent the transfer of water and heat through the soil based on a multilayer diffusion scheme, as well as plant growth and leaf-scale physiological processes. ISBA models key vegetation variables like LAI and above ground biomass, the diurnal cycle of water, carbon and energy fluxes. It computes a soil-vegetation composite using a single-source energy budget. In the CO2-responsive version of ISBA, ISBA-A-gs, the model can simulate the CO2 net assimilation and GPP by considering the functional relationship between the photosynthesis rate (A) and the stomatal aperture (gs) based on the biochemical A-gs model proposed by Jacob et al., 1996. Photosynthesis is in control of the evolution of vegetation variables. It makes vegetation growth possible as a result of an uptake of CO2. Oppositely, a deficit of photosynthesis triggers higher mortality rates. Ecosystem respiration (RECO) is represented by the CO2 being released by the soil-plant system and GPP by the carbon uptake related to photosynthesis. Finally, the net ecosystem exchange (NEE) consists of the difference between GPP and RECO. Each ISBA grid

cell is composed of up to 12 generic land surface types, bare soil, rocks, and permanent snow and ice surfaces as well as nine plant functional types (needle leaf trees, evergreen broadleaf trees, deciduous broadleef trees, C3 crops, C4 crops, C4 irrigated crops, herbaceous, tropical herbaceous and wetlands). The ECOCLIMAP-II land cover database (Faroux et al., 2013) provides ISBA parameters for each patch and each grid cell.

ISBA multilayer diffusion scheme's default discretization is 14 layers over 12 m depth. The following configuration is used in this study: thickness (depth) of each layers are (from top to bottom), 1 cm (0-1 cm), 3 cm (1-4 cm), 6 cm (4-10 cm), 10 cm (10-20 cm), 20 cm (20-40 cm), 20 cm (40-60 cm), 20 cm (60-80 cm), 20 cm (80-100 cm), 50 cm (100-150cm), 50 cm (150-200cm), 100 cm (200-300 cm), 200 cm (300-500 cm), 300 cm (500-800 cm) and 400 cm (800 to 1200 cm), see also Figure 1 of Decharme et al., 2011. Snow is represented using the ISBA 12-layers explicit snow scheme (Boone and Etchevers, 2001, Decharme et al., 2016).

2.1.2 CTRIP river routing system

The ISBA-CTRIP river routing system is able to simulate continental scale hydrological variables based on a set of three prognostic equations. They correspond to (i) the groundwater, (ii) the surface stream water and (iii) the seasonal floodplains. It converts the runoff simulated by ISBA into river discharge. ISBA-CTRIP river-routing network has a spatial resolution of 0.5° x 0.5° globally and is coupled daily with ISBA through the OASIS3-LCT coupler (Voldoire et al., 2017). ISBA provides to CTRIP updated fields of runoff, drainage, groundwater and floodplain recharges. In turn, CTRIP provides ISBA with water table depth, floodplain fraction as well as flood potential infiltration so that ISBA can simulate capillarity rise, evaporation and infiltration over flooded areas. A comprehensive overview of how CTRIP is coupled with ISBA is available in Decharme et al., (2019).

2.1.3 Data assimilation

The SEKF used in LDAS-Monde is a 2-step sequential approach in which a forecast step is followed by an analysis step. The forecast step propagates the initial state of the studied system to the next time step with the ISBA LSM and then, the analysis step corrects this forecast by assimilating observations. The flow-dependency (dynamic link) between the prognostic variables and the observations is ensured in the SEKF through the observation operator and its Jacobians, which propagate information from the observations to the analysis via finite-difference computations (de Rosnay et al., 2013). The Jacobian matrix has as many rows as assimilated observation types (in our case two: SSM and LAI) and as many columns as model control variables requested (in our case eight, soil moisture from layers 2 to 8, 1-100cm, and LAI). In addition to a

control run (i.e. the forecast step), computing the Jacobian matrix requires perturbed runs, one for each control variable. The eight control variables are directly updated using their sensitivity to observed variables (i.e. defined by the Jacobian). Other variables are indirectly modified through biophysical processes and feedback from the model. Several studies (e.g. Draper et al., 2009; Rüdiger et al., 2010) have demonstrated that small perturbations lead to a good approximation of this linear behaviour, provided that computational round-off error is not significant. Typically, for those runs, the initial state of the control variable is perturbed by about 0.1% (see Albergel et al., 2017; Rüdiger et al., 2010). The length of the LDAS-Monde assimilation window is 24 hours . A mean volumetric standard deviation error is specified proportional to the soil moisture range (the difference between the volumetric field capacity and the wilting point, calculated as a function of the soil type, as given by Noilhan et Mahfouf, 1996) and scaled by a factor 0.04 for SSM in its model equivalent (the second layer of soil between 1 and 4 cm), and 0.02 for deeper layers (soil layers 3 to 8, 4-100 cm). The observational SSM error follows the same rule scaled by 0.05 and is consistent with errors typically expected for remotely sensed SSM (e.g., de Jeu et al., 2008, Gruber et al, 2016). Based on previous results from Jarlan et al., 2008, Rüdiger et al., 2010, Barbu et al., 2011, observed LAI standard deviation errors are set to 20 % of the LAI value itself. Modelled LAI standard deviation errors follow the same rule for values higher than 2 m^2m^{-2}. For values lower than 2 m^2m^{-2}, a fixed value of 0.04 m^2m^{-2} has been used. More detailed can be found in Barbu et al., 2011 (section 2.3 on data assimilation scheme and figure 2).

2.2 Atmospheric forcing

The lowest model level (about 10 metres above ground level) of air temperature, wind speed, specific humidity and pressure, the downwelling fluxes of shortwave, longwave radiations as well as precipitation (partitioned in solid and liquid phases) are needed to force LDAS-Monde. In this study, LDAS-Monde is driven by several near-surface meteorological fields from ECMWF:

- its most recent atmospheric reanalysis (ERA5) to produce LDAS-Monde global analysis
- its high resolution Integrated Forecast System (IFS HRES) to monitor and predict the evolution of LSVs for regions under severe droughts and heatwaves.

ERA5 (Hersbach et al., 2018, 2019 submitted) is the fifth generation of global reanalyses produced by ECWMF. This atmospheric reanalysis is a key element of the Copernicus Climate Change Service (C3S) and is available from 1979 onward (data is released about 2 months behind real time). ERA5 has hourly output analysis, 31 km horizontal dimension and 137 levels in the vertical resolution. Several studies have validated the ERA5 dataset. For example, Urraca et al. (2018) have compared incoming solar radiation from both ERA5 and the ERA-interim reanalysis (Dee et al.,

2011) at a global scale and found evidence that ERA5 outperforms ERA-Interim. In another study, Beck et al. (2019) have highlighted the good performance of ERA5 precipitation with respect to a set of 26 gridded (sub-daily) precipitation data sources by comparing them to Stage-IV gauge-radar data over the CONUS domain (CONtinental United States of America). Tall et al. (2019) have used in situ measurements of precipitation at more than 100 stations spanning all over Burkina-Faso in Western Africa as well as incoming solar radiation from 4 in situ stations to evaluate the quality of ERA5 over ERA-Interim with positive outcomes for ERA5 as well. They have also evaluated both reanalysis datasets through their impact on the representation of LSVs when used to force the ISBA LSM, again demonstrating a clear advantage for ERA5. Similar work has been done by Albergel et al. (2018a), over North America, this study found enhanced performances in the representation of evapotranspiration, snow depth, soil moisture as well as river discharge when the ISBA LSM was forced by ERA5 compared to ERA-Interim.

At the time of the study, ERA5 underlying model and data assimilation system (Cycle 41r2) are very similar to that of the operational weather forecast, HRES, which has production cycles ranging from 41r2 to 45r1 during the study period (the cycle is 46r1 from June 2019, more information at https://www.ecmwf.int/en/forecasts/documentation-and-support/changes-ecmwf-model, last accessed July 2019). The main difference between ERA5 and HRES over the considered period is the horizontal resolution, 9 km in HRES and 31 km in ERA5. The atmospheric forcing is interpolated from the native grids of ERA5 and HRES to regular grids of 0.25° × 0.25° and 0.1° × 0.1°, respectively, using a bilinear interpolation from the native grid to the regular grid. ERA5 and HRES were used in Albergel et al. (2019) to force LDAS-Monde in order to study the impact of the 2018 summer heatwave in Europe. Authors have highlighted that the HRES configuration exhibits better monitoring skills than the coarser resolution ERA5 configuration.

In forecasting mode, HRES forecast is also available everyday from 00:00 UTC with a 10-day lead time, but with changes in the temporal resolution. HRES forecast step frequency is hourly up to time step 90 (i.e. day 3), 3-hourly from time-step 90 to 144 (i.e. day 6) and 6-hourly from time-step 144 to 240 (i.e. day 10). In this study, for forecast experiments (see section 2.4 for details on the experimental setup) HRES forecasts with a 10-day lead time are used to drive forecasts of the LSVs from LDAS_HRES open-loop and analysis configurations in order to evaluate the impact of the initialisation on the forecast of LSVs. The original 3-hourly time steps are used up to day 6 (time step 144), the 6-hourly time steps from day 6 to 10 are interpolated to 3-hourly frequency to avoid discontinuities.

2.3 Assimilated satellite Earth Observations

Two types of satellite-derived variables are assimilated in LDAS-Monde: ASCAT Soil Water Index (SWI) and LAI GEOV1. They are both freely available through the Copernicus Global Land Service (CGLS, https://land.copernicus.eu/global/index.html, last accessed June 2019).

ASCAT stands for Advanced Scatterometer, this is an active C-band microwave sensor that is onboard the European MetOp polar orbiting satellites (METOP-A, from 2006, B from 2012 and also C from 2018). From ASCAT radar backscatter coefficients, it is possible to derive information on SSM following a change detection approach (Wagner et al., 1999, Bartalis et al., 2007). The recursive form of an exponential filter (Albergel et al., 2008), is then applied to estimate the SWI using a timescale parameter, T (varying between 1 day and 100 days) T is a surrogate parameter for all the processes potentially affecting the temporal dynamics of soil moisture (like, soil hydraulic properties and thickness of the soil layer, evaporation, run-off and vertical gradient of soil properties such as texture and density). The obtained SWI then ranges between 0 (dry) and 100 (wet). In this study, CGLS SWI-001 (i.e. produced with a T-value of 1 day) is used as a proxy for SSM (Kidd et al., 2013). Grid points with an average altitude exceeding 1500 m above sea level as well as those with more than 15 % of urban land cover are rejected as those conditions are known to affect the retrieval of SSM from space. Prior to the assimilation, SSM has to be converted from the observation space to the model space. This is done through a linear rescaling as proposed by Scipal et al. (2007), where the mean and variance of observations are matched to the mean and variance of the modelled soil moisture from the second layer of soil (1-4 cm depth). This rescaling gives in practice very similar results to CDF (cumulative distribution function) matching. The linear rescaling is performed on a seasonal basis (with a 3-month moving window) as suggested by Draper et al., (2011), Barbu et al., (2014).The LAI GEOV1 observations are based on data from both SPOT-VGT (up to 2014) and PROBA-V (from 2014) satellites. They span from 1999 to present, have a 1km x 1km spatial resolution and are produced according to the methodology developed by Baret et al. (2013). LAI GEOV1 observations have a temporal frequency of 10 days at best (in the presence of clouds, no observation is available). LAI data are masked in the presence of modelled snow by the ISBA LSM.

As in previous studies (e.g, Barbu et al., 2014, Albergel et al., 2019), observations are interpolated by an arithmetic average to the model grid points (0.25° or 0.10° in this study), if at least 50 % of the model grid points are observed (i.e. half the maximum amount). ASCAT SSM and LAI GEOV1 are illustrated by Figure 1.

2.4 Experimental setup

LDAS-Monde is first run at a global scale, at 0.25° x 0.25° spatial resolution, forced by ERA5 atmospheric reanalysis and assimilating SSM and LAI EOs from 2010 to 2018 (LDAS_ERA5 hereafter). LDAS_ERA5 is spun-up by running year 2010 twenty times. LDAS_ERA5 analysis as well as its model counterpart (open-loop, i.e. no data assimilation) are presented and evaluated in this study.

This 9-yr global reanalysis is then used to provide a monthly climatology for estimating anomalies of the land surface conditions. For each month (and variable considered) of 2018 we have removed the monthly mean and scaled by the monthly standard deviation of the 2010-2018 period. Significant anomalies are used to trigger more detailed monitoring as well as forecasting activities for a region of interest. 19 regions across the globe known for being potential hot spots for droughts and heatwaves have been selected. They are listed in Table I and presented in Figure 2. Monthly anomalies of LDAS_ERA5 analysis of SSM and LAI for those 19 regions are assessed for 2018 (with respect to the 2010-2018 period) and regions presenting significant level of negative anomalies are selected and further investigated. For those regions, LDAS-Monde has been driven by HRES atmospheric analysis leading to a 0.1° x 0.1° analysis of the LSVs from April 2016 to December 2018 (LDAS_HRES herafter). HRES is available at a 0.1° x 0.1° resolution only from April 2016. April to December 2016 is used as a short period for spin-up and results are presented for the period 2017-2018. Although a 9-month spin-up period can be seen as rather short, evaluating LDAS-HRES on either 2017-2018 or 2018 (using instead a 21-month spin-up) leads to similar results on surface soil moisture and LAI (not shown). While the system is not fully spun-up, it can be considered as representative of the system response to data assimilation. LDAS_HRES complements the coarser spatial resolution LDAS_ERA5. HRES forecasts with a 10 day lead time are also used, and initialised by either LDAS_HRES open-loop or analysis (LDAS_Fc hereafter) in order to assess the impact of the initialisation on the forecast. Forecasts with a four and height day lead time are presented, only (LDAS_fc4 and LDAS_fc8, respectively). A summary of the experimental setup is given in Table II.

2.5 Evaluation datasets and metrics

This study uses several satellite-derived estimates of EOs as well as in situ measurement data. LDAS_ERA5 analysis impact is assessed with respect to the open-loop model run (i.e. no assimilation). The two assimilated datasets, CGLS SSM and LAI, are used to verify to which extent the assimilation system is able to correctly integrate them (i.e. suggesting a healthy behaviour from the data assimilation system). Then several spatially distributed datasets independent from both experiments: (namely) evapotranspiration from the GLEAM project (Miralles et al., 2011, Martens

et al., 2017, version 3b entirely satellite driven), GPP from the FLUXCOM project (Tramontana et al., 2016, Jung et al., 2017), SIF from the GOME-2 (Global Ozone Monitoring Experiment-2) scanning spectrometer (Munro et al., 2006, Joiner et al., 2016) and snow cover data from the Interactive Multi-sensor Snow and Ice Mapping System (or IMS, https://www.natice.noaa.gov/ims/) are used in the evaluation process. The IMS snow cover product combines ground observations and satellite data from microwave and visible sensors (using geostationary and polar orbiting satellites) to provide snow cover information in all weather conditions. The IMS product is available daily for the northern hemisphere.

In situ measurements of surface soil moisture from 19 networks across 14 countries available from the ISMN are also used to evaluate the performance of the soil moisture analysis. They represent 782 stations with at least 2 years of daily data over 2010-2018. Sensors at 5 cm depth (SSM) are compared with soil moisture from LDAS_ERA5 third layer of soil (4-10 cm), sensors at 20 cm depth with the fourth layer of soil (10-20 cm, 685 stations from 10 networks). Beside 11 stations located in 4 countries of Western Africa (Benin, Mali, Sénégal and Niger) and 21 stations in Australia, most of the station are located in North America and Europe, see Table S3. Evaluation datasets are listed in Table III along with the metrics used. For satellite datasets of SWI, LAI, evapotranspiration and GPP, correlations (R), Root Mean Square Differences (RMSD) and Normalized RMSD (N_{RMSD}, Eq.(1)) are used as metrics. .

$$N_{RMSD} = \frac{RMSD_{(\text{Analysis})} - RMSD_{(\text{Model})}}{RMSD_{(\text{Model})}} \times 100 \qquad \text{Eq.(1)}$$

Regarding the SIF satellite dataset, fluorescence is not simulated directly in the ISBA LSM. However, photosynthesis activity is simulated through the calculation of the GPP, which is driven by plant growth and mortality in the model. Modelled GPP values are expressed in $g(C)\cdot m^{-2}\cdot day^{-1}$, while SIF is an energy flux emitted by the vegetation ($mW\cdot m^{-2}\cdot sr^{-1}\cdot nm^{-1}$). Hence, GPP and SIF cannot be directly compared as they do not represent the same physical quantities. However, several studies (e.g, Zhang et al., 2016, Sun et al., 2017, Leroux et al., 2018) have found that their time dynamics investigated, highlighting the potential of SIF products to be used as a validation support for GPP models. Therefore, correlation between modelled GPP and observed SIF is used as metrics. About the snow cover dataset, differences between observed and modelled snow cover is considered for the evaluation.

For in situ datasets of soil moisture and evapotranspiration, usual correlation, RMSD, unbiased RMSD and bias are considered as metrics. Moreover, a Normalized Information Contribution (NIC, Eq.(2)) measure is applied to the correlation values to quantify the improvement or degradation due to the specific configuration.

$$\mathrm{NIC}_R = \frac{R_{(\mathrm{Analysis})} - R_{(\mathrm{Model})}}{1 - R_{(\mathrm{Model})}} \times 100 \qquad \text{Eq. (2)}$$

NIC scores are classified according to three categories: (i) negative impact from the analysis with respect to the open-loop with values smaller than -3 %, (ii) positive impact from the analysis with respect to the open-loop with values greater than +3 % and (iii) neutral impact from the analysis with respect to the open-loop with values between -3 % and 3 %.

In addition, for surface soil moisture, correlation is calculated for both absolute (R) and anomaly ($R_{anomaly}$) time-series in order to remove the strong impact from the SSM seasonal cycle on this specific metric (see e.g. Albergel et al. , 2018a, 2018b).

Finally, the Nash-Sutcliffe Efficiency score (NSE, Eq.(3), Nash and Sutcliffe, 1970) is used to evaluate LDAS_ERA5 experiments ability to represent the monthly discharge dynamics.

$$\mathrm{NSE} = 1 - \frac{\sum_{mt=1}^{T} \left(Q_s^{mt} - Q_o^{mt}\right)^2}{\sum_{mt=1}^{t} \left(Q_s^{mt} - \overline{Q_s^{mt}}\right)^2} \qquad \text{Eq.(3)}$$

where Q_s^{mt} is the monthly river discharge from LDAS_ERA5 (analysis or open-loop) at month *mt*, and Q_o^{mt} is the observed river discharge at month *mt*. NSE can vary between $-\infty$ and 1. An exact match between model predictions and observed data is defined as a value of 1, whereas a value of 0 means that the model predictions have the same accuracy as the mean of the observed data. Finally negative values represent situations where the observed mean is a better predictor than the model simulation. NIC presented in Eq.(1) has also been applied to NSE scores to assess the added value of LDAS_ERA5 analysis over its open-loop counterpart. Stations with NSE values lesser that -2 have been discarded. A similar threshold has already been used in previous studies evaluating LDAS-Monde (e.g. Albergel et al., 2017, 2018a). Many processes, most of them linked to water management such as the presence of dams and reservoirs, irrigation, water uptake in urban areas, are not yet represented in ISBA possibly leading to a poor representation of river discharges. As previous evaluations studies have suggested a neutral to positive impact from the assimilation, only, it has been decided to focus on stations with reasonable NSE values.

3 Global assessment of LDAS_ERA5

3.1 Gridded datasets

In this sub-ection, LDAS-Monde open-loop and analysis are first compared to the assimilated observations (SSM and LAI) to demonstrate that the assimilation system is working as intended. Both experiments are also compared to independent sources of information to evaluate the analysis

impact (GPP, EVAP and SIF). Figure 3 presents mean RMSD values between the observations and LDAS_ERA5 for the open-loop (Figure 3a), and for the analysis (Figure 3b) for LAI over 2010-2018. Because LAI observations are ingested into the model, the assimilation reduces the LAI RMSD values almost everywhere. It can be noted that rather large LAI RMSD values (> 1.5 m^2m^{-2}) can remain in some areas after the assimilation, especially in densely forested areas. Figure 4 illustrates latitudinal plots of LAI, SSM, GPP and EVAP for LDAS_ERA5 before assimilation (the open-loop) and after assimilation (the analysis) along with observations. The number of points considered per latitudinal stripes of 0.25° is represented, also. From Figure 4a it is possible to see the positive impact the analysis has on LAI compared to the open-loop, with the former being closer to the observations. Improvements from the analysis occurs from nearly 80°North to about 55° South, areas around the equator are particularly improved. This demonstrates that the data assimilation system is working as intended. A smaller impact than for LAI is obtained for SSM, GPP and EVAP, hardly visible at this scale. The mean latitudinal results show a consistent difference in terms of GPP and EVAP between LDAS_ERA5 and the observational products. These differences are systematic with higher values in tropical regions. Figure 5 represents latitudinal plots of score differences (correlations and normalized RMSD) for LAI, SSM, GPP, EVAP and SIF. For SIF only differences in correlation are represented as it is used to evaluate GPP variability as in Leroux et al., 2018. Score differences are computed as follow, analysis minus open-loop using monthly averages over 2010-2018 for LAI and SSM, 2010-2013 for GPP, 2010-2016 for EVAP and 2010-2015 for SIF. For each panel of Figure 5, the vertical dashed line represents the 0-value. For plots of correlation differences, positive values indicate an improvement from the analysis with respect to the open-loop simulation. Similarly, for plots of RMSD differences, negative values indicate an improvement from the analysis with respect to the open-loop simulation. LAI and SSM being assimilated variables, the analysis leads to a clear improvement in both correlation and RMSD. Such improvement is expected and reflects the healthy behaviour of the assimilation system. Both variables are improved at almost all latitudes with the exception around 45°S for LAI correlation values (very few land points). For SSM a noticeable improvement in both correlation and RMSD is found around 20°N corresponding mainly to an improvement in the Sahara desert (not shown). Being linked to LAI, GPP is also improved across almost all latitudes (to a lesser extend than LAI) with a particularly positive impact below 20°N. As seen on Figure 5 d) and i), there is little impact on variable EVAP which can be considered negligible. It highlights the difficulty of land surface data assimilation to impact model fluxes by modifying model states.

Panels of Figure 6 illustrate histograms of score differences (correlation and RMSD, analysis minus open-loop) for LAI, SSM, GPP, EVAP and SIF. The Number of available data as well as the

425 percentage of positive and negative values are reported. For correlations (RMSD) differences, positive (negative) values indicate an improvement from the analysis over the open-loop. Regarding LAI, the analysis improves 96.9% of the grid points for correlations and 99.9% for N_{RMSD}. As for SSM, correlation values are improved for 92.8% of the grid points (92.4% for R_{MSD}). When using independent datasets such as GPP and SIF, one may also notice an improvement from
430 the analysis, correlation (N_{RMSD}) are better for 81.1% (74.1%) and 79.7% (for SIF N_{RMSD} is not applicable) of the grid points. Results using the GLEAM dataset for evapotranspiration are more contrasted with 63.6% (48.9%) of the grid points showing an improvement from the analysis. I It is worth mentioning that 24.9% (39.6%) of the grid point shows a decrease in skill. However, GLEAM is an evaporation model designed to be driven by remote sensing observations only.
435 GLEAM only estimates (root-zone) soil moisture and terrestrial evaporation while the CO2-responsive version of ISBA in LDAS_ERA5 is a physically-based land surface model, accounting for more processes linked to vegetation (see section 2.1.1). It has to be noted that the auxiliary dataset used to e.g. represent the different land cover types are different also. Within GLEAM, the land cover types fractions are sourced from the Global Vegetation Continuous Fields product
440 (MOD44B), based on observations from the Moderate Resolution Image Spectroradiometer (MODIS). Four land cover types are considered, bare soil, low vegetation (e.g. grass), tall vegetation (e.g. trees), and openwater (e.g. lakes). In ISBA the 12 land cover types fraction depart from prevalent land cover products such as CLC2000 (Corine Land Cover) and GLC2000 (Global Land Cover). It can potentially impact the distribution of the terrestrial evaporation between
445 GLEAM and ISBA. Further work at CNRM will focus on understanding the differences between ISBA and GLEAM, in particular investigating the sub-components of terrestrial evaporation.

Finally, Figure S1 and Figure S2 illustrate snow cover evaluation. LDAS_ERA5 snow cover is evaluated against the IMS snow cover (as e.g. in Orsolini et al., 2019). Figure S1 shows the averaged northern hemisphere snow cover fraction for the 2010-2018 period. It is complemented by
450 all panels of Figure S2 showing (i) maps of IMS snow cover (top row) for 3 seasons, September-October-November (SON), December-January-February (DJF) and March-April-May (MAM), respectively, (ii) maps of snow cover from LDAS_ERA5 open-loop (second row), (iii) maps of snow cover differences between the open-loop and IMS data and (iv) maps of snow cover differences between the analysis and the open-loop. LDAS_ERA5 open-loop compares very well
455 with the IMS snow-cover data in the accumulation season from September to February (Figure S2 and panels d) to i) of Figure S1), only with an overestimation over the Tibetan Plateau. The issue over Tibet from ERA5 is not new, and consistent with previous studies like Orsolini et al., 2019. An early melt in spring compared to observations is noted in LDAS_ERA5 and could be related with

the snow cover parametrization in ISBA. As expected, the analysis has an almost neutral impact on snow as both SSM and LAI observations are filtered out from frozen/snow condition and as there is no snow data assimilation yet in LDAS_ERA5 (Figure S2 and panels (j), (k) and (l) of Figure S1). This clearly shows, however an area of potential improvement of data assimilation within LDAS-Monde using satellite data such as the IMS one (as in e.g. de Rosnay et al., 2014).

3.2 Ground-based datasets

LDAS_ERA5 analysis and open-loop are also evaluated using independent in situ measurements of evapotranspiration, river discharge and surface soil moisture across the world. Daily in situ measurements of evapotranspiration from the FLUXNET-2015 synthesis data set (http://fluxnet.fluxdata.org/, last accessed June 2019) are first used in this study. The LDAS_ERA5 ability to represent evapotranspiration is evaluated using correlation (R), RMSD and ubRMSD as well as bias (LDAS_ERA5 minus observations) using the 85 selected FLUXNET-2015 stations. Median R, RMSD, ubRMSD and bias for LDAS_ERA5 analysis (open-loop) are 0.73 (0.72), 28.74 (29.60) $W.m^{-2}$, 27.37 (26.92) $W.m^{-2}$ and 4.64 (4.40) wm^{-2}, respectively. If these numbers depict a small advantage of the analysis over the open-loop configuration, it is worth mentioning that differences are rather small and likely to fall within the uncertainty of the in situ measurement.

Figure 7(a) represents the added value of the analysis based on NIC_R (Eq.(2)), large blue circles represent a positive impact from the analysis (20 stations) with a NIC_R greater than +3 (i.e. R values are better when the analysis is used than when the model is used) while large red circles represent a degradation from the analysis (5 stations) with a NIC_R smaller than -3. Stations with a rather neutral impact (60 stations) with a NIC_R between [-3 ; +3] are reported using small dots. Note that at the scale of Figure 7(a), some stations are overlapping. Figure 7(a) is complemented by panels (b), (c), (d) and (e) that are scatter-plots of R, ubRMSD, absolute bias and RMSD between LDAS_ERA5 analysis (x-axis), open-loop (y-axis) for the 85 stations from the Fluxnet2015, 56 stations (out of 85) have better R values considering the analysis. They are 41 for ubRMSD, 47 for RMSD and 44 for absolute bias. The set of 20 stations from Figure 7(a) where the analysis has a positive impact at NIC_R greater than +3 are reported in green on Figure 7(b).

Results on river discharge are illustrated by Figure 8 (panels a and b). Figure 8(a) represents NSE scores for the subset of 982 stations selected. Most of them are located in North America and Europe while a few are available in South America and Africa. Figure 8(a) is complemented by Figure 8(b)that represents the NIC score applied to NSE score and emphasizes the added value of LDAS_ERA5 analysis over the open-loop. 74% of this subset of stations presents a rather neutral impact from the analysis (with a NIC ranging between -3% and +3%) while 26% (254 stations) presents a significant impact (with a NIC above +3% or below -3%) . When the analysis impacts the

representation of river discharge, this impact tends to be positive with 74% (189 stations) having a NIC score greater than 3% while only 26% (65 stations) presents NIC score smaller than -3%.

The statistical scores for soil moisture from LDAS_ERA5 open-loop and analysis (third and fourth layers of soil, 4-10 cm depth, 10-20 cm depth, respectively) over 2010-2018 when compared with ground measurements from the ISMN (5 cm depth and 20 cm depth, respectively) are presented in Table S3 for each individual network. Averaged statistical metrics (ubRMSD, R, $R_{anomaly}$ and bias) are similar for both LDAS_ERA5 analysis and open-loop even if local differences exist. For the analysis, averaged R ($R_{anomaly}$) values along with its 95% Confidence Interval (CI) using in situ measurements at 5 cm (782 stations from 19 networks) are 0.68±0.03 (0.53±0.04) (0.67±0.03 (0.53±0.04) for the open-loop) with averaged-network values going up to 0.88±0.01 (0.58±0.04) for the analysis (SOILSCAPE network, 49 stations in the USA) and always higher than 0.55 except for one network, ARM (10 stations in the USA) presenting an averaged R value of 0.29±0.05. Averaged ubRMSD and bias (LDAS_ERA5 minus in situ) are 0.060 m^3m^{-3} and 0.077 m^3m^{-3} for the analysis, 0.060 m^3m^{-3} and 0.076 m^3m^{-3} for the open-loop, respectively. NIC (Eq.2) has also been applied to R values, 65% of the pool of stations present a neutral impact from the analysis (511 stations at NIC ranging between -3 and +3), 12% present a negative impact (91 stations at NIC < -3) and 23% present a positive impact at (180 stations at NIC > +3).

The number of stations where R differences between the analysis and the open-loop are significant (i.e. their 95% CI are not overlapping) is 186 out of 782 (about 26%). There is an improvement from the analysis w.r.t. the open-loop for 128 stations (out of 186, i.e. about 69%) and a degradation for 58 stations (about 31%). Figure 9 illustrates R differences between the analysis and the open-loop runs over CONUS where most of the stations are located (552 out of 782). When differences (analysis minus openloop) are not significant stations are represented by a small dot (425 stations out of 552, about 77%). When they are significant (127 stations out of 552, about 23%), large circles have been used, blue for positive differences (an improvement from the analysis, 99 stations out of 127, about 78%) and red for negative differences (a degradation from the analysis, 28 stations, about 22%). For most of the stations where a significant difference is obtained, it represent an improvement from the analysis.

Averaged analysis R (95%CI), bias and ubRMSD for the fourth layer of soil (685 stations from 10 networks) are 0.65±0.03, 0.049 m^3m^{-3} and 0.055 m^3m^{-3}, respectively. For the open-loop, they are 0.64±0.03, 0.048 m^3m^{-3} and 0.056 m^3m^{-3}, respectively. For soil moisture at that depth, about 60% of the stations present a neutral impact from the analysis (410 stations at NIC ranging between -3 and +3), 28% a positive impact (189 stations at NIC > +3) and 12% a negative impact (86 stations at NIC < -3). Although differences between the open-loop run and the analysis are rather small, these

results underline the added value of the analysis with respect to the model run. Figure S3 represents the distribution of the scores values for LDAS_ERA5 open-loop and analysis using boxplots centred on the median value. They look very similar and from Figure S3, it is difficult to see either improvement or degradation from the analysis.

For evapotranspiration, river discharge and surface soil moisture there is a slight advantage for LDAS_ERA5 analysis with respect to its open-loop counterpart. Even if the distribution of the averaged statistical metrics can be rather similar for both (particularly true for surface soil moisture evaluation), there are significant regional differences for some sites, which shows the added value of the analysis with respect to the open-loop.

4. Monitoring and forecasts for areas under severe/extreme conditions

4.1 Selection of two regional case studies

For each individual region presented in Table I and Figure 2, monthly anomalies (scaled by the standard deviation) of analysed SSM (second layer of soil, 1-4cm) and LAI for 2018 are assessed with respect to the 2010-2018 period. The anomalies (see Figure 10) highlight three regions, two presenting strong negative anomalies for both SSM and LAI for almost all 2018 (North Western Europe, WEUR, and the Murray-Darling basin, MUDA, in South Eastern Australia) and one presenting strong positive anomalies of SSM and LAI in Eastern Africa (EAFR). WEUR and MUDA regions were affected by a severe heatwave and a drought in 2018 impacting LSVs analysed by LDAS_ERA5. According to Figure 10, monthly anomalies of SSM and LAI for MUDA are negative through the whole 2018 with 7 and 6 months presenting LAI and SSM anomalies below -1 standard deviation (stdev), respectively. WEUR has negative SSM anomalies from May to December 2018 with values going below -2 stdev. LAI was severely impacted as well with July to October 2018 presenting negative anomalies below -2 stdev. For WEUR, 5 months present LAI and SSM anomalies below -1 stdev. EAFR experiences 3 and 7 months with positive anomalies for SSM and LAI in 2018 above 1 stdev (8 and 7 months consecutively present positive anomalies for SSM and LAI respectively).

According to the National Oceanic and Atmospheric Administration (NOAA), Europe experienced its warmest summer since continental records began in 1910 at +2.16°C above mean (Global Climate Report, https://www.ncdc.noaa.gov/sotc/global/ last accessed April 2019). In Europe, temperature for the whole summer 2018 was above climatology. The summer 2018 heatwave in Europe has already reported in the scientific literature (e.g. Magnusson et al., 2018, Albergel et al., 2019, Blyverket et al., 2019).

In its 70th Special Climate Statement, the Australian Bureau of Meteorology (BoM) has reported a very hot and dry summer 2018 in eastern Australia (BoM, 2019). Like much of Australia, the Murray Darling basin has experienced a remarkably dry and hot weather during 2018. The annual maximum temperature for the Murray Darling basin as a whole was more than two degrees above average during 2018. The northern Murray–Darling Basin in particular was severely affected with inflows to all catchments persistently well below average (http://www.bom.gov.au/state-of-the-climate/, last visited: April 2019). Finally, the East Africa Seasonal Monitor based on the Famine Early Warning System Network (FEWS) confirms above-average rainfall amounts as well as significantly greener than normal vegetation conditions (e.g., https://reliefweb.int/report/somalia/east-africa-seasonal-monitor-july-27-2018, last visited: April 2019). As this study focuses on monitoring and forecasting the impact of severe droughts conditions on LSVs, WEUR and MUDA are selected for further investigation.

4.2 Case studies presentation: LDAS-Monde medium resolution (0.25° x 0.25°) experiments

Figure 11 illustrates seasonal cycles of observed LAI (Figure 11a) and SWI (Figure 11e), LDAS_ERA5 analysis and open-loop LAI (Figure 11b) and SSM (Figure 11f) for the WEUR domain. 2018 is compared to an average of the period 2010-2017. From Figure 11a, one may see the heatwave impact with a sharp drop in observed LAI values from June to November 2018 (solid green line). Such low LAI values have never been observed over the eight previous years (dashed green line for the 2010-2017 averaged along with the 2010-2017 minimum and maximum observations in shaded green). A similar behaviour is also visible in the ASCAT SWI dataset in Figure 11e with the lowest values ever reached in this 2010-2018 period. Over WEUR, LDAS_ERA5 open-loop overestimates LAI in the second part of the year as already highlighted by several studies (e.g. Albergel et al., 2017, 2019). LDAS_ERA5 analysis has a positive impact, reducing LAI values, as seen on Figure 11b (LAI open-loop in blue, analysis in red) Panels c), d) g) and h) of Figure 11) depict a similar situation for the MUDA area, almost every month of 2018 presents the lowest values for both SSM and LAI. For both MUDA and WEUR, the smaller differences for LAI and SSM between LDAS_ERA5 analysis and open-loop in 2018 compared to 2010-2017 also suggest that both extreme events were well captured in the atmospheric forcing used to drive LDAS_ERA5.

4.3 Case studies for assessing LDAS-Monde high resolutions (0.1° x 0.1°) analysis and forecast experiments

For these two specific areas (WEUR and MUDA), LDAS-Monde is also run forced by HRES (LDAS_HRES) at 0.1° x 0.1° spatial resolution over April 2016 to December 2018. Additionally to

LDAS_HRES analysis, forecast experiments with a lead time of 4-days and 8-days, initialised by either LDAS_HRES analysis or open-loop are presented for 2017-2018 (for SSM and LAI) in order to assess the impact of the initial conditions on the forecast of the LSVs. In this subsection, this new set of six experiments is verified against the assimilated observations. Verification of the forecast experiments can be viewed as an independent validation as those observations are not assimilated yet. It is worth mentioning that there is a difference between the use of SSM and LAI observations to evaluate the forecast. For SSM, the assimilation is done after a rescaling to the model climatology (see section 2.3), which removes bias. For LAI, however this is not the case and the assimilation process unbiases the modelled LAI (w.r.t. the observation). This difference, together with the longer memory of LAI (compared SSM), contributes to the results presented in this sub-section. Statistical scores for LDAS_HRES open-loop and analysis are presented, also, to serve as a benchmark of the forecast experiments.

Upper panels of Figure 12 (for WEUR) and Figure 13 (for MUDA), illustrate seasonal RMSD (Figure 12a, 13a) and correlation (Figure 12b, 13b) values between SSM from the second layer of soil (1–4 cm) from LDAS-Monde forced by HRES (LDAS_HRES, open-loop and analysis) and ASCAT SSM estimates over 2017-2018. Scores between SSM from the second layer of soil of LDAS_HRES 4-day forecast (LDAS_fc4, initialised by either the open-loop or analysis) and 8-day forecast (LDAS_fc8, initialised by either the open-loop or analysis) and ASCAT SSM estimates are reported, also. From the upper panels of those figures one may notice a small improvement from the analysis (solid red line) over the open-loop simulation (solid blue line), slightly decreasing RMSD values and increasing correlations values. However no improvement (nor degradation) is visible from the 4-d and 8-d forecasts experiments initialised by LDAS_HRES analysis over those initialised by LDAS_HRES open-loop, they display very similar scores. LDAS_HRES SSM is of better quality than LDAS_fc4 and LDAS_fc8. Note however that for the MUDA area, there is a small positive impact of the initialisation on the 4-d and 8-d forecast of surface soil moisture (Figure 13a, b). Those results suggest that this fast evolving model variable (SSM between 1 cm and 4 cm depth) relies more on the atmospheric forcing than on the initial conditions (at least within the forecast range presented in this study) and it can be assumed that the 4-day and 8-day atmospherical forecast from HRES is of lower quality that the first 24-h analysis. Results for LAI are different from SSM (lower panels of Figure 12 and Figure 13). Firstly, there is a large improvement from the analysis (solid red line) over the open-loop (solid blue line), particularly in the LAI decaying phase (Boreal and Austral autumns mainly). Secondly, LDAS_HRES open-loop (solid blue line), LDAS_fc4 (dotdashed blue line) and LDAS_fc8 (dashed blue line) initialised by LDAS_HRES open-loop present very similar skills, so do LDAS_fc4 and LDAS_fc8 initialised by

LDAS_HRES analysis (dotdashed and dashed red lines, respectively). They also outperform skills of LDAS_HRES open-loop, LDAS_fc4 and LDAS_fc8 initialised by LDAS_HRES open-loop. This suggests that LAI relies more on its initial conditions than on the atmospheric forcing (at least within the forecast range presented in this study) and that forecasting LAI is also a matter of initial conditions. This statement is valid for these two contrasted areas, WEUR and MUDA.

These results are corroborated by Figures 14 (for WEUR) and 15 (for MUDA), top rows illustrate SSM and bottom rows LAI. Figures 14(a) and 15(a) show RMSD values between LDAS_HRES open-loop SSM (1-4 cm) and ASCAT SSM over 2017-2018 for the WEUR and MUDA domains, respectively. Due to the seasonal linear rescaling applied to ASCAT estimates, RMSD values are rather small. For the WEUR (MUDA) domain they range from 0 to 0.048 m^3m^{-3} (0 to 0.040 m^3m^{-3}). Figures 14(b) and 15(b) represent maps of RMSD differences between LDAS_HRES analysis (open-loop) and ASCAT SSM estimates over 2017-2018 for the WEUR and MUDA domains, as well. Both maps are dominated by negative values (in blue) indicating that RMSD values are smaller (better) when using LDAS_HRES analysis than when using LDAS_HRES open-loop. It is also worth-mentioning than no positive differences (i.e. a degradation from the analysis) are present in those maps. For the MUDA domain, they are improved by about 15%. Figures 14(c), (d) 15(c), (d) are also maps of RMSD differences, they consider forecast experiments (LDAS_fc4, LDAS_fc8). It appears that for both domains, the impact from the initialisation is rather small with few coloured areas, strengthening previous results suggesting that, forcing quality is more important than initial conditions to forecast SSM variable. Results are different for LAI, RMSD values for LDAS_HRES open-loop are ranging between 0 and 1.6 m^2m^{-2} over WEUR, 0 and 1 m^2m^{-2} over MUDA (Figures 14(e) and 15(e)). RMSD values are improved by up to 37 % over WEUR and up to 60% over MUDA by the analysis (Figures 14(f) and 15(f)). Improvement from the analysis over the open-loop experiment is consistent through all the WEUR domain while the improvement over the MUDA domain is restrained to the south eastern part (the north western part has low RMSD values as the open-loop).

Similarly to Figures 14(a, b, c, d) panels of Figure 16 illustrates the impact of the analysis on SSM using correlations. This time, ASCAT SWI (i.e. no rescaling) has been used. Figure 16 (top panels) shows map of R values based on absolute values while Figure 16 (bottom panels) shows R values on anomalies (short term variability) as defined in Albergel et al., 2018a. Figure 16 (a) and (e) represents R values and anomaly R values for LDAS_HRES, respectively. As expected R values are higher than anomaly R values. Maps of differences (panels b and f) of Figure 16 suggest that after assimilation, both scores are improved rather equally. While the 4 day and 8-day forecast still show an improvement from the initial condition on R values (panels c and d of Figure 16 dominated by

positive differences, analysis minus open-loop), maps of anomaly R values forecast do not display any negative or positive impact (panels g and h of Figure 16).

Finally, top panels of Figure 17 illustrate the impact of the analysis on drainage monitoring and forecast over WEUR. Fig. 17 a) represents drainage from LDAS_HRES open-loop varying between 0 and 1 $kg.m^{-2}.day^{-1.}$ Fig.17 b) shows the drainage difference between LDAS_HRES analysis and openloop. The analysis impact on drainage is rather small, about ±3% and more pronounced in areas where the analysis has affected LAI more (see panels f), g) and h) of Figure 14). As seen on panels c) and d), there is also an impact from the initialisation in areas were the analysis was more effectively correcting LAI. Bottom panels of Figure 17 illustrate a similar impact on runoff. As for drainage, this variable is affected by the analysis. Initial conditions have an impact on its forecast, also. Although we did not present a quality assessment of those two variables, our findings on river discharge analysis impact, but also those from Albergel et al., 2017, 2018a, suggest a neutral to positive impact, propagated from the analysis of SSM and LAI to river discharge through variables such as drainage and runoff.

5. Discussion and conclusion

This study has demonstrated that combining a LSM, satellite EOs and atmospheric forcing through LDAS-Monde has a great potential to represent the impact of extreme weather (heatwaves and droughts) on land surface conditions. LDAS-Monde is now ready for use in various applications such as (i) reanalyses of land Essential Climate Variables (ECVs), (ii) monitoring of water resources, drought and vegetation, and (iii) detection of severe conditions over land and initialisation of LSVs forecast. It has been applied in this study to past events of 2018 with respect to a short period of time (2010-2018) as a demonstrator but will be extended to a longer time period. LDAS-Monde operational use in near real time has the capacity to serve as an emergency monitoring system for the LSVs. Using atmospheric reanalysis like ERA5 to force LDAS-Monde guarantees a high level of consistency because of its frozen configuration (no changes in spatial and vertical resolutions, data assimilation and parametrizations). The ERA5 coarse spatial resolution makes it affordable to run long term and large scale LDAS-Monde experiments. With ERA5 available from 1979 and now covering near real-time needs with its ERA5T version (https://climate.copernicus.eu/climate-reanalysis), an LDAS_ERA5 configuration would be able to provide a long term and near real time coarse resolution (0.25° x 0.25°) climatology as reference for anomalies of the land surface conditions. Significant anomalies could then be used to trigger more focused “on-demand” simulations for regions experiencing extreme conditions. In that case LDAS-Monde could be run forced by e.g. ECMWF operational high resolution product (0.10° x 0.10°) in

monitoring and forecast (up to 10-d ahead) modes, as was presented here for two regions in North Western Europe and South Eastern Australia. In term of RMSD, our results showed a very small impact of initial conditions on the forecasts of SSM. This was expected due to the reduced memory of the top soil surface (1-4 cm), which is dominated by meteorological variability. However, the LAI initialisation had significant impact on the LAI forecast skill. This was also expected due to the memory of vegetation evolution. For SSM, the assimilation is done after a rescaling to the model climatology (see section 2.3), which removes bias. For LAI, however this is not the case and the assimilation process removes bias in the modelled LAI (w.r.t. the observation). This technical difference between SSM and LAI assimilation, combined with the longer memory of LAI compared to SSM, contributes to the results presented in this study. Despite the expected behaviour of these two LSVs in forecasting, our results show that LDAS-Monde system is capable of propagating the initial LAI conditions, which is relevant not only for LSV medium-range forecasting but with potential for longer lead-times. The strong impact of LAI initialisation on the forecast does not seem to propagate to surface soil moisture and further studies are necessary to test the impact of initial conditions to additional variables from LDAS-Monde (including soil moisture in deeper layers and evapotranspiration). Another possibility would be to force LDAS-Monde using ECMWF ensemble forecasts, although the ensemble system has coarser spatial-resolution (~0.20° x 0.20°), it offers a 15-day forecast and a 51 member ensemble, which can introduce forcing uncertainty into the LSVs. The maximum range of the soil and vegetation forecast could even reach up to six months if using seasonal atmospheric forecasts as forcing.

LDAS-Monde has well identified areas of developments that can further improve the representation of LSVs. For instance, it does not consider snow data assimilation yet and it has been shown in this study that if the snow accumulation seems to be represented correctly in the system, it suffers from a too early snow-melt in spring time. To overcome this issue, two possibilities will be explored. Firstly using a recently developed ISBA parametrisation, MEB for Multiple Energy Budget which is known to lead to a better representation of the snowpack (Boone et al., 2017), in particular in the densely forested areas of the Northern Hemisphere where large differences between LDAS-Monde and the IMS snow cover were found in spring (Figure S2(i), Aaron Boone CNRM, personal communication June 2019) and (ii) adapting the current data assimilation scheme of LDAS-Monde to permit assimilation the IMS snow cover data (as done e.g. at ECMWF, de Rosnay et al., 2014). The current SEKF data assimilation scheme is also being revisited. Even though it has provided good results, one of its limitations is the computation of a Jacobian matrix which needs one model run for each control variable, requiring significant computational resources with increased number of control variables. That is why more flexible Ensemble based approaches like the Ensemble

Square Root Filter (EnSRF) have recently been implemented (Fairbain et al., 2015, Bonan et al., 2020). Bonan et al., 2020 have evaluated performances from the EnSRF and the SEKF over the Euro-Mediterranean area. Both data assimilation schemes have a similar behaviour for LAI while for SSM, EnSRF estimates tend to be closer to observations than those from the SEKF. They have also conducted an independent evaluation of both assimilation approaches using satellite estimates of evapotranspiration and GPP as well as measures of river discharges from gauging stations. They have found that the EnSRF leads to a systematic (moderate) improvement for evapotranspiration and GPP and a highly positive impact on river discharges, while the SEKF lead to more contrasting performance. As for applications in hydrology, the 0.5° x 0.5° spatial resolution TRIP river network is currently being improved to 1/12° x 1/12° globally.

CNRM is also investigating the direct assimilation of ASCAT radar backscatter (Shamambo et al., 2019), it is supposed to tackle the way vegetation is accounted for in the change detection approach used to retrieve SSM with an improved representation of its effect. Assimilating ASCAT radar backscatter also raises the question of how to specify observation, background, and model error covariance matrices, so far mainly relying on soil properties (see section 2.1.3 on data assimilation). The last decade has seen the development of techniques to estimate those matrices. Approaches based on Desroziers diagnostics (Desroziers et al., 2005) are affordable for land data assimilation systems from a computational point of view and could provide insightful information on the various sources of the data assimilation system.

Also, the added value of LDAS-Monde compared to already existing datasets has to be evaluated and current work at Météo-France is investigating its quality against state of the art reanalyses such as those from NASA at either global scale (GLDAS, Rodell et al., 2004, MERRA-2, The Modern-Era Retrospective Analysis for Research and Applications, Version 2, Reichle et al., 2017, Draper et al., 2018) or regional scale (NCALDAS over the continental USA, FLDAS over Africa). Finally, first attempts to go to higher spatial resolution over smaller areas like the AROME domain (Applications de la Recherche à l'Opérationnel à Méso-Echelle, https://www.umr-cnrm.fr/spip.php?article120, last accessed July 2019) of Météo-France (centred over France) at kilometre scale and assimilating kilometric and sub-kilometric scale satellite retrieval of SSM and LAI (from CGLS) are very promising.

Code availability. LDAS-Monde is a part of the ISBA land surface model and is available as open source via the surface modelling platform called SURFEX. SURFEX can be downloaded freely at http: //www.umr-cnrm.fr/surfex/ using a CECILL-C Licence (a French equivalent to the L-GPL licence; http://www.cecill.info/licences/Licence_CeCILL-C_V1-en.txt). It is updated at a relatively

low frequency (every 3 to 6 months). If more frequent updates are needed, or if what is required is not in Open-SURFEX (DrHOOK, FA/LFI formats, GAUSSIAN grid), you are invited to follow the procedure to get a SVN account and to access real-time modifications of the code (see the instructions at the first link). The developments presented in this study stemmed on SURFEX version 8.1. LDAS-Monde technical documentation and contact point are freely available at: https://opensource.umr-cnrm.fr/projects/openldasmonde/files

Data availability: upon request by contacting the corresponding author.

Author Contributions: Conceptualization, CA, JCC.; Investigation, CA, YZ, BA, SM, NRF; Methodology, CA; Writing—original draft, CA, BA; Writing—review and editing, All

Funding: This research was funded by IRT Antoine de Saint-Exupéry Foundation, grant number CDT-R056-L00-T00 (POMME-V project), the Climate Change Initiative Programme Extension, Phase 1 - Climate Modeling User Group ESA/contract No 4000125156/18/I-NB

.

Acknowledgments: Results were generated using the Copernicus Climate Change Service Information, 2017. The Authors would like to thanks the Copernicus Global Land Service for providing the satellite derived Leaf Area Index and Surface Soil Moisture.

Conflicts of Interest: The authors declare no conflict of interest

References

Albergel, C.; Rüdiger, C.; Pellarin, T.; Calvet, J.-C.; Fritz, N.; Froissard, F.; Suquia, D.; Petitpa, A.; Piguet, B.; Martin, E. From near-surface to root-zone soil moisture using an exponential filter: An assessment of the method based on in-situ observations and model simulations. Hydrol. Earth Syst. Sci., 12, 1323–1337, 2008.

Albergel, C., Munier, S., Leroux, D. J., Dewaele, H., Fairbairn, D., Barbu, A. L., Gelati, E., Dorigo, W., Faroux, S., Meurey, C., Le Moigne, P., Decharme, B., Mahfouf, J.-F., and Calvet, J.-C.: Sequential assimilation of satellite-derived vegetation and soil moisture products using SURFEX_v8.0: LDAS-Monde assessment over the Euro-Mediterranean area, Geosci. Model Dev., 10, 3889–3912, https://doi.org/10.5194/gmd-10-3889-2017, 2017.

Albergel, C.; Munier, S.; Bocher, A.; Bonan, B.; Zheng, Y.; Draper, C.; Leroux, D.J.; Calvet, J.-C. LDAS-Monde Sequential Assimilation of Satellite Derived Observations Applied to the Contiguous US: An ERA5 Driven Reanalysis of the Land Surface Variables. Remote Sens., 10, 1627, 2018a

Albergel, C.; Dutra, E.; Munier, S.; Calvet, J.-C.; Munoz-Sabater, J.; de Rosnay, P.; Balsamo, G. ERA-5 and ERA-Interim driven ISBA land surface model simulations: Which one performs better? Hydrol. Earth Syst. Sci., 22, 3515–3532, 2018b.

Albergel, C.; Dutra, E.; Bonan, B.; Zheng, Y.;Munier, S.; Balsamo, G.; de Rosnay, P.;Muñoz-Sabater, J.; Calvet, J.-C. Monitoring and Forecasting the Impact of the 2018 Summer Heatwave on Vegetation. Remote Sens., 11, 520, 2019.

Balsamo, G., Albergel, C., Beljaars, A., Boussetta, S., Brun, E., Cloke, H., Dee, D., Dutra, E., Muñoz-Sabater, J., Pappenberger, F., de Rosnay, P., Stockdale, T., and Vitart, F.: ERA-Interim/Land: a global land surface reanalysis data set, Hydrol. Earth Syst. Sci., 19, 389-407, https://doi.org/10.5194/hess-19-389-2015, 2015.

Balsamo, G.; Agusti-Panareda, A.; Albergel, C.; Arduini, G.; Beljaars, A.; Bidlot, J.; Bousserez, N.; Boussetta, S.; Brown, A.; Buizza, R.; Buontempo, C.; Chevallier, F.; Choulga, M.; Cloke, H.; Cronin, M.F.; Dahoui, M.; De Rosnay, P.; Dirmeyer, P.A.; Dutra, M.D.E.; Ek, M.B.; Gentine, P.; Hewitt, H.; Keeley, S.P.E.; Kerr, Y.; Kumar, S.; Lupu, C.; Mahfouf, J.-F.; McNorton, J.; Mecklenburg, S.; Mogensen, K.; Muñoz-Sabater, J.; Orth, R.; Rabier, F.; Reichle, R.; Ruston, B.; Pappenberger, F.; Sandu, I.; Seneviratne, S.I.; Tietsche, S.; Trigo, I.F.; Uijlenhoet, R.; Wedi, N.; Woolway, R.I.; Zeng, X. Satellite and In Situ Observations for Advancing Global Earth Surface Modelling: A Review. *Remote Sens.*, *10*(12), 2038; https://doi.org/10.3390/rs10122038, 2018.

Bamzai, A.; Shukla, J. Relation between Eurasian snow cover, snow depth and the Indian summer monsoon: An observational study. J. Clim., 12, 3117–3132, 1999.

Barbu, A.L.; Calvet, J.-C.; Mahfouf, J.-F.; Albergel, C.; Lafont, S. Assimilation of Soil Wetness Index and Leaf Area Index into the ISBA-A-gs land surface model: Grassland case study. Biogeosciences, 8, 1971–1986., 2011.

Barbu, A. L., Calvet, J.-C., Mahfouf, J.-F., and Lafont, S.: Integrating ASCAT surface soil moisture and GEOV1 leaf area index into the SURFEX modelling platform: a land data assimilation application over France, Hydrol. Earth Syst. Sci., 18, 173–192, https://doi.org/10.5194/hess-18-173-2014, 2014.

Barella-Ortiz, A. and Quintana-Seguí, P.: Evaluation of drought representation and propagation in Regional Climate Model simulations over Spain, Hydrol. Earth Syst. Sci. Discuss., https://doi.org/10.5194/hess-2018-603, in review, 2018.

Baret, F.; Weiss, M.; Lacaze, R.; Camacho, F.; Makhmarad, H.; Pacholczyk, P.; Smetse, B. GEOV1: LAI, FAPAR essential climate variables and FCOVER global time series capitalizing over existing products, Part 1: Principles of development and production. Remote Sens. Environ. , 137, 299–309, doi:10.1016/j.rse.2012.12.027, 2013.

Bartalis, Z.; Wagner, W.; Naeimi, V.; Hasenauer, S.; Scipal, K.; Bonekamp, H.; Figa, J.; Anderson, C.: Initial soil moisture retrievals from the METOP-A advanced Scatterometer (ASCAT). Geophys. Res. Lett., 34, L20401, doi: 10.1029/2007GL031088., 2007.

Bauer, P.; Thorpe, A.; Brunet, G. The quiet revolution of numerical weather prediction. Nature, 525, 47–55, doi:10.1038/nature14956, 2015.

Beck, H. E., Pan, M., Roy, T., Weedon, G. P., Pappenberger, F., van Dijk, A. I. J. M., Huffman, G. J., Adler, R. F., and Wood, E. F.: Daily evaluation of 26 precipitation datasets using Stage-IV gauge-radar data for the CONUS, Hydrol. Earth Syst. Sci., 23, 207–224, https://doi.org/10.5194/hess-23-207-2019, 2019.

Bell, J. E., M. A. Palecki, C. B. Baker, W. G. Collins, J. H. Lawrimore, R. D. Leeper, M. E. Hall, J. Kochendorfer, T. P. Meyers, T. Wilson, and H. J. Diamond.: U.S. Climate Reference Network soil moisture and temperature observations. J. Hydrometeorol., 14, 977-988. doi: 10.1175/JHM-D-12-0146.1, 2013.

Bierkens, M.; van Beek, L. Seasonal predictability of European discharge: Nao and hydrological response time. J. Hydrometeorol, 10, 953–968, 2009.

Blyverket, J.; Hamer, P.D.; Schneider, P.; Albergel, C.; Lahoz, W.A. Monitoring Soil Moisture Drought over Northern High Latitudes from Space. *Remote Sens.*, *11*, 1200, 2019.

Bonan, B., Albergel, C., Zheng, Y., Barbu, A. L., Fairbairn, D., Munier, S., and Calvet, J.-C.: An ensemble square root filter for the joint assimilation of surface soil moisture and leaf area index within the Land Data Assimilation System LDAS-Monde: application over the Euro-Mediterranean region, Hydrol. Earth Syst. Sci., 24, 325–347, https://doi.org/10.5194/hess-24-325-2020, 2020.

Boone, A.; Masson, V.; Meyers, T.; Noilhan, J. The influence of the inclusion of soil freezing on simulations by a soil-vegetation-atmosphere transfer scheme. J. Appl. Meteorol., 39, 1544–1569, 2000.

Boone, A. and Etchevers, P.: An intercomparison of three snow schemes of varying complexity coupled to the same land-surface model: local scale evaluation at an Alpine site, J. Hydrometeo-rol., 2, 374–394, 2001.

Boone, A., Samuelsson, P., Gollvik, S., Napoly, A., Jarlan, L., Brun, E., and Decharme, B.: The interactions between soil–biosphere–atmosphere land surface model with a multi-energy balance (ISBA-MEB) option in SURFEXv8 – Part 1: Model description, Geosci. Model Dev., 10, 843-872, https://doi.org/10.5194/gmd-10-843-2017, 2017.

Bruce, J.P., Natural disaster reduction and global change. Bulletin of the American Meteorological Society, 75(10): 1831–1835, 1994.

Bureau of Meteorology Special Climate Statement 70: Drought conditions in eastern Australia and impact on water resources in the Murray–Darling Basin, Issued 9 April 2019, http://www.bom.gov.au/climate/current/statements/scs70.pdf, 2019.

Calvet, J.-C.; Noilhan, J.; Roujean, J.-L.; Bessemoulin, P.; Cabelguenne, M.; Olioso, A.; Wigneron, J.-P. An interactive vegetation SVAT model tested against data from six 780 contrasting sites. Agric. For. Meteorol, 92, 73–95, 1998.

Calvet, J.-C.; Rivalland, V.; Picon-Cochard, C.; Guehl, J.-M. Modelling forest transpiration and CO2 fluxes—Response to soil moisture stress. Agric. For. Meteorol, 124, 143–156, 2004.

Cook, E.R., Seager, R., Cane, M.A. and Stahle, D.W., North American drought: reconstructions, causes, and consequences. Earth Science Reviews, 81(1): 93–134, 2007.

de Jeu, R.A.; Wagner, W.; Holmes, T.R.H.; Dolman, A.J.; Van De Giesen, N.C.; Friesen, J. Global soil moisture patterns observed by space borne microwave radiometers and scatterometers. Surv. Geophys., 29, 399–420, 2008.

de Rosnay, P. A simplified Extended Kalman Filter for the global operational soil moisture analysis at ECMWF. Q. J. R. Meteorol. Soc., 139, 1199–1213, doi: 10.1002/qj.2023, 2013.

de Rosnay, P.; Balsamo, G.; Albergel, C.; Muñoz-Sabater, J.; Isaksen, L. Initialisation of land surface variables for numerical weather prediction. Surv. Geophys., 35, 607–621, doi: 10.1007/s10712-012-9207-x, 2014.

Desroziers, G.; Berre, L.; Chapnik, B.; Poli, P. Diagnosis of observation, background and analysis-error statistics in observation space. Q. J. Roy. Meteor. Soc., 131, 3385–3396, 2005.

Di Napoli, C., F. Pappenberger, and H.L. Cloke: Verification of Heat Stress Thresholds for a Health-Based Heat-Wave Definition. *J. Appl. Meteor. Climatol.,* **58**, 1177–1194, https://doi.org/10.1175/JAMC-D-18-0246.1, 2019.

Decharme, B., Boone, A., Delire, C., and Noilhan, J.: Local evaluation of the Interaction between soil biosphere atmosphere soil multilayer diffusion scheme using four pedotransfer functions, J. Geophys. Res., 116, D20126, https://doi.org/10.1029/2011JD016002, 2011.

Decharme, B.; Martin, E.; Faroux, S. Reconciling soil thermal and hydrological lower boundary conditions in land surface models. J. Geophys. Res. Atmos., 118, 7819–7834, 2013.

Decharme, B., Brun, E., Boone, A., Delire, C., Le Moigne, P., and Morin, S.: Impacts of snow and organic soils parameterization on northern Eurasian soil temperature profiles simulated by the ISBA land surface model, The Cryosphere, 10, 853–877, https://doi.org/10.5194/tc-10-853-2016, 2016.

Decharme, B., Delire, C., Minvielle, M., Colin, J., Vergnes, J.-P., Alias, A., Saint-Martin, D., Séférian, R., Sénési, S. and Voldoire, A.: Recent changes in the ISBA-CTRIP Land Surface System for use in the CNRM-CM6 climate model and in global off-line hydrological applications, J. Adv. Model Earth Sy., 11, 1207-1252, 10.1029/2018MS001545, 2019.

Dee, D.P.; Uppala, S.M.; Simmons, A.J.; Berrisford, P.; Poli, P.; Kobayashi, S.; Andrae, U.; Balmaseda, M.A.; Balsamo, G.; Bauer, D.P. The ERA-Interim reanalysis: Configuration and performance of the data assimilation system. Q. J. R. Meteorol. Soc., 137, 553–597, 2011.

Dirmeyer, P. A., Gao, X., Zhao, M., Guo, Z., Oki, T., and Hanasaki N.: The Second Global Soil Wetness Project (GSWP-2): Multi-model analysis and implications for our perception of the land surface, B. Am. Meteorol. Soc., 87, 1381–1397, https://doi.org/10.1175/BAMS-87-10-1381, 2006.

Dorigo, W. A., Wagner, W., Hohensinn, R., Hahn, S., Paulik, C., Xaver, A., Gruber, A., Drusch, M., Mecklenburg, S., van Oevelen, P., Robock, A., and Jackson, T.: The International Soil Moisture Network: a data hosting facility for global in situ soil moisture measurements, Hydrol. Earth Syst. Sci., 15, 1675-1698, https://doi.org/10.5194/hess-15-1675-2011, 2011.

Dorigo, W.A., A. Gruber, R.A.M. De Jeu, W. Wagner, T. Stacke, A. Loew, C. Albergel, L. Brocca, D. Chung, R.M. Parinussa and R. Kidd: Evaluation of the ESA CCI soil moisture product using ground-based observations, Remote Sensing of Environment, http://dx.doi.org/10.1016/j.rse.2014.07.023, 2015.

Draper, C. S., Mahfouf, J.-F., and Walker, J. P.: An EKF assimilation of AMSR-E soil moisture into the ISBA land surface scheme, J. Geophys. Res., 114, D20104, https://doi.org/10.1029/2008JD011650, 2009.

Draper, C.; Mahfouf, J.-F.; Calvet, J.-C.; Martin, E.; Wagner, W. Assimilation of ASCAT near-surface soil moisture into the SIM hydrological model over France. Hydrol. Earth Syst. Sci., 15, 3829–3841, 2011.

Draper, C. S., R. H. Reichle, and R. D. Koster, Assessment of MERRA-2 Land Surface Energy Flux Estimates, Journal of Climate, 31, 671-691, doi:10.1175/JCLI-D-17-0121.1, 2018.

Faroux, S.; Kaptué Tchuenté, A.T.; Roujean, J.-L.; Masson, V.; Martin, E.; Moigne, P.L. ECOCLIMAP-II/Europe: A twofold database of ecosystems and surface parameters at 1 km resolution based on satellite information for use in land surface, meteorological and climate models. Geosci. Model Dev., 6, 563–582, 2013.

Fairbairn, D., Barbu, A. L., Mahfouf, J.-F., Calvet, J.-C. and Gelati, E.: Comparing the ensemble and extended Kalman filters for in situ soil moisture assimilation with contrasting conditions, Hydrol. Earth Syst. Sci., 19, 4811–4830, doi: 10.5194/hess-19-4811-2015, 2015.

Fairbairn, D.; Barbu, A.L.; Napoly, A.; Albergel, C.; Mahfouf, J.-F.; Calvet, J.-C. The effect of satellite-derived surface soil moisture and leaf area index land data assimilation on streamflow simulations over France. Hydrol. Earth Syst. Sci., 21, 2015–2033, 2017.

Fox, A.M.; Hoar, T.J.; Anderson, J.L.; Arellano, A.F.; Smith, W.K.; Litvak, M.E.; MacBean, N.; Schimel, D.S.; Moore, D.J.P. Evaluation of a Data Assimilation System for Land Surface Models using CLM4.5. J. Adv. Model. Earth Syst., 10, 2471–24942, 2018.

Gibelin, A.-L.; Calvet, J.-C.; Roujean, J.-L.; Jarlan, L.; Los, S.O. Ability of the land surface model ISBA-A-gs to simulate leaf area index at global scale: Comparison with satellite products. J. Geophys. Res., 111, 1–16, 2006.

Gruber, A.; Su, C.-H.; Zwieback, S.; Crow, W.; Dorigo, W.; Wagner, W. Recent advances in (soil moisture) triple collocation analysis. Int. J. Appl. Earth Obs. Geoinf., 45, 200–211, 2016.

Hersbach, H., de Rosnay, P. Bell, B., Schepers, D., Simmons, S., Soci, S., Abdalla, S., Alonso Balmaseda, M., Balsamo, G., Bechtold, P., Berrisford, P., Bidlot, J., de Boisséson, E., Bonavita, M., Browne, P., Buizza, R., Dahlgren, P., Dee, D., Dragani, R., Diamantakis, M., Flemming, J., Forbes, R., Geer, A., Haiden, T., Hólm, E., Haimberger, L., Hogan, R., Horányi, A., Janisková, M., Laloyaux, P., Lopez, P., Muñoz-Sabater, J., Peubey, C., Radu, R., Richardson, D., Thépaut, J.-N., Vitart, F., Yang, X., Zsótér, E. and Zuo H. Operational global reanalysis: Progress, future directions and synergies with NWP. ERA Rep. Ser., 27, 65., 2018.

Hersbach, H., B. Bell, P. Berrisford, S. Hirahara, A. Horanyi, J. Muñoz-Sabater, J. Nicolas, C. Peubey, R. Radu, D. Schepers, A. Simmons, C. Soci, S. Abdalla, X. Abellan, G. Balsamo, P. Bechtold, G. Biavati, J. Bidlot, M. Bonavita, G. De Chiara, P. Dahlgren, D. Dee, M. Diamantakis, R. Dragani, J. Flemming, R. Forbes, M. Fuentes, A. Geer, L. Haimberger, S. Healy, R. J. Hogan, E. Holm, M. Janiskova, S. Keeley, P. Laloyaux, P. Lopez, G. Radnoti, P. de Rosnay, I. Rozum, F. Vamborg, S. Villaume, J.-N. Thépaut: The ERA5 Global Reanalysis, QJRMS, submitted, 2019

IPCC: Managing the Risks of Extreme Events and Disasters to Advance Climate Change Adaptation. A Special Report of Working Groups I and II of the Intergovernmental Panel on Climate Change . Cambridge University Press, Cambridge, UK, and New York, NY, USA, 582 pp, 2012.

IPCC: Climate change 2014: Synthesis Report. Contribution of Working Groups I, II and III to the Fifth Assessment Report of the Intergovernmental Panel on Climate Change [Core Writing Team, R.K. Pachauri and L.A. Meyer (eds.)]. IPCC, Geneva, Switzerland, 151 pp, 2014.

Jacobs, C.M.J.; van den Hurk, B.J.J.M.; de Bruin, H.A.R. Stomatal behaviour and photosynthetic rate of unstressed grapevines in semi-arid conditions. Agric. For. Meteorol. 80, 111–134, 1996.

Jarlan, L., Balsamo, G., Lafont, S., Beljaars, A., Calvet, J.-C., and Mougin, E.: Analysis of leaf area index in the ECMWF land surface model and impact on latent heat on carbon fluxes: Application to West Africa, J. Geophys. Res., 113, D24117, doi:10.1029/2007JD009370, 2008.

Joiner, J.; Yoshida, Y.; Guanter, L.; Middleton, E.M. New methods for the retrieval of chlorophyll red fluorescence from hyperspectral satellite instruments: Simulations and application to GOME-2 and SCIAMACHY. Atmos. Meas. Tech. 2016, 9, 3939–3967, 2016.

Jung, M., Reichstein, M., Schwalm, C. R., Huntingford, C., Sitch, S., Ahlström, A., Arneth, A., Camps-Valls, G., Ciais, P., Friedlingstein, P., Gans, F., Ichii, K., Jain, A. K., Kato, E., Papale, D., Poulter, B., Raduly, B., Rödenbeck, C., Tramontana, G., Viovy, N., Wang, Y.-P., Weber, U., Zaehle, S., and Zeng, N.: Compensatory water effects link yearly global land CO2 sink changes to temperature, Nature, 541, 516–520, https://doi.org/10.1038/nature20780, 2017.

Ionita, M., Tallaksen, L. M., Kingston, D. G., Stagge, J. H., Laaha, G., Van Lanen, H. A. J., Scholz, P., Chelcea, S. M., and Haslinger, K.: The European 2015 drought from a climatological perspective, Hydrol. Earth Syst. Sci., 21, 1397-1419, https://doi.org/10.5194/hess-21-1397-2017, 2017.

Kaminski, T. Assimilating atmospheric data into a terrestrial biosphere model: A case study of the seasonal cycle. Glob. Biogeochem. Cycles, 16, 2002.

Kidd, R.; Makhmara, H.; Paulik, C. GIO GL1 PUM SWI I1.00.pdf., p. 25. Available online: http://land.copernicus.eu/global/ products/SWI/Documents/ProductUserManual (accessed on 1 June 2019), 2013.

Kumar, S.V., B.F. Zaitchik, C.D. Peters-Lidard, M. Rodell, R. Reichle, B. Li, M. Jasinski, D. Mocko, A. Getirana, G. De Lannoy, M.H. Cosh, C.R. Hain, M. Anderson, K.R. Arsenault, Y. Xia, and M. Ek: Assimilation of Gridded GRACE Terrestrial Water Storage Estimates in the North American Land Data Assimilation System. *J. Hydrometeor.,* **17**, 1951–1972, https://doi.org/10.1175/JHM-D-15-0157.1, 2016

Kumar, S.V.; Jasinski, M.; Mocko, D.; Rodell, M.; Borak, J.; Li, B.; Kato Beaudoing, H.; Peters-Lidard, C.D. NCA-LDAS land analysis: Development and performance of a multisensor, multi-variate land data assimilation system for the National Climate Assessment. J. Hydrometeorol., doi:10.1175/JHM-D-17-0125.1., 2018.

Kumar, S.V., D.M. Mocko, S. Wang, C.D. Peters-Lidard, and J. Borak, 0: Assimilation of remotely sensed Leaf Area Index into the Noah-MP land surface model: Impacts on water and carbon fluxes and states over the Continental U.S.. J. Hydrometeor., https://doi.org/10.1175/JHM-D-18-0237.1., 2019.

Koster, R.D.; Mahanama, S.P.P.; Livneh, B.; Lettenmaier, D.P.; Reichle, R.H. Skill in stremflow forecasts derived from large-scale estimates of soil moisture and snow. Nat. Geosci. Lett., 3, 613–616, 2010.

Lahoz, W.; De Lannoy; G. Closing the gaps in our knowledge of the hydrological cycle over land: Conceptual problems. Surv. Geophys., 35, 577–606, 2014.

Leroux, D.J.; Calvet, J.-C.; Munier, S.; Albergel, C. Using Satellite-Derived Vegetation Products to Evaluate LDAS-Monde over the Euro-Mediterranean Area. Remote Sens., 10, 1199, 2014.

Luo, L.; Wood, E.F. Monitoring and predicting the 2007 U.S. drought. Geophysical Research Letters, 34. doi:10.1029/2007GL031673, 2007.

Magnusson, L.; Ferranti, L.; Vamborg, F. Forecasting the 2018 European heatwave. ECMWF Newslett., 157, 4, 2018.

Mahfouf, J.-F.; Bergaoui, K.; Draper, C.; Bouyssel, F.; Taillefer, F.; Taseva, L. A comparison of two off-line soil analysis schemes for assimilation of screen level observations. J. Geophys. Res., 114, D08105, 2009.

Martens, B., Miralles, D. G., Lievens, H., van der Schalie, R., de Jeu, R. A. M., Fernández-Prieto, D., Beck, H. E., Dorigo, W. A., and Verhoest, N. E. C.: GLEAM v3: satellite-based land evaporation and root-zone soil moisture, Geosci. Model Dev., 10, 1903–1925, https://doi.org/10.5194/gmd-10-1903-2017, 2017.

Massari, C.; Camici, S.; Ciabatta, L.; Brocca, L. Exploiting Satellite-Based Surface Soil Moisture for Flood Forecasting in the Mediterranean Area: State Update Versus Rainfall Correction. Remote Sens., 10, 292, 2018.

Masson, V., Le Moigne, P., Martin, E., Faroux, S., Alias, A., Alkama, R., Belamari, S., Barbu, A., Boone, A., Bouyssel, F., Brousseau, P., Brun, E., Calvet, J.-C., Carrer, D., Decharme, B., Delire, C., Donier, S., Essaouini, K., Gibelin, A.-L., Giordani, H., Habets, F., Jidane, M., Kerdraon, G., Kourzeneva, E., Lafaysse, M., Lafont, S., Lebeaupin Brossier, C., Lemonsu, A., Mahfouf, J.-F., Marguinaud, P., Mokhtari, M., Morin, S., Pigeon, G., Salgado, R., Seity, Y., Taillefer, F., Tanguy, G., Tulet, P., Vincendon, B., Vionnet, V., and Voldoire, A.: The SURFEXv7.2 land and ocean surface platform for coupled or offline simulation of earth surface variables and fluxes, Geosci. Model Dev., 6, 929–960, https://doi.org/10.5194/gmd-6-929-2013, 2013.

McNally, A., Arsenault, K., Kumar, S., Shukla, S., Peterson, P., Wang, S., Funk, C., Peters-Lidard, C.P., Verdin, J.P. A land data assimilation system for sub-Saharan Africa food and water security applications. Sci. Data 4:170012 https://doi.org/10.1038/sdata.2017.12, 2017

Mishra, A.K. and Singh, V.P., A review of drought concepts. Journal of Hydrology, 391(1): 202–216, 2010.

Miralles, D.G., De Jeu, R.A.M., Gash, J.H., Holmes, T.R.H., Dolman, A.J., Magnitude and variability of land evaporation and its components at the global scale. Hydrol. Earth Syst. Sci. 15 (3), 967–981. http://dx.doi.org/10.5194/hess-15-967-2011, 2011.

Nash, J. E. and Sutcliffe, V.: River forecasting through conceptual models, J. Hydrol., 10, 282–290, 1970.

Noilhan, J. and Planton, S.: A simple parameterization of land surface processes for meteorological models. Mon. Weather Rev., 117, 536–549, doi: 10.1175/1520-0493(1989)117<0536%3AASPOLS>2.0.CO%3B2, 1989.

Noilhan, J.; Mahfouf, J.-F. The ISBA land surface parameterisation scheme. Glob. Planet. Chang., 13, 145–159, 1996

Muñoz□Sabater, J. , Lawrence, H. , Albergel, C. , de Rosnay, P. , Isaksen, L. , Mecklenburg, S. , Kerr, Y. and Drusch, M., Assimilation of SMOS brightness temperatures in the ECMWF Integrated Forecasting System. Q J R Meteorol Soc. Accepted Author Manuscript. doi:10.1002/qj.3577, 2019.

Munro, R.; Eisinger, M.; Anderson, C.; Callies, J.; Corpaccioli, E.; Lang, R.; Lefebvre, A.; Livschitz, Y.; Perez Albinana, A. GOME-2 on MetOp: From In-Orbit Verification to Routine Operations. In Proceedings of the EUMETSAT Meteorological Satellite Conference, Helsinki, Finland, 12–16 June 2006.

Obasi, G.O.P., WMO's role in the international decade for natural disaster reduction. Bulletin of the American Meteorological Society, 75(9): 1655–1661, 1994.

Orsolini, Y., Wegmann, M., Dutra, E., Liu, B., Balsamo, G., Yang, K., de Rosnay, P., Zhu, C., Wang, W., and Senan, R.: Evaluation of snow depth and snow-cover over the Tibetan Plateau in global

reanalyses using in-situ and satellite remote sensing observations, The Cryosphere Discuss., https://doi.org/10.5194/tc-2019-49, in review, 2019.

Reichle, R.H.; Koster, R.D.; Liu, P.; Mahanama, S.P.P.; Njoku, E.G.; Owe, M. Comparison and assimilation of global soil moisture retrievals from the Advanced Microwave Scanning Radiometer for the Earth Observing System (AMSR-E) and the Scanning Multichannel Microwave Radiometer (SMMR). J. Geophys. Res., 112, D09108, doi:10.1029/2006JD008033, 2007.

Reichle, R. H., C. S. Draper, Q. Liu, M. Girotto, S. P. P. Mahanama, R. D. Koster, and G. J. M. De Lannoy, Assessment of MERRA-2 land surface hydrology estimates, Journal of Climate, 30, 2937-2960, doi:10.1175/JCLI-D-16-0720.1, 2017.

Reichle, R. H., Liu, Q., Koster, R. D., Crow, W. T., De Lannoy, G. J. M., Kimball, J. S., Ardizzone, J.V., Bosch, D., Colliander, A., Cosh, M., Kolassa, J., Mahanama, S.P., Prueger, J., Starks, P., Walker, J.P., Version 4 of the SMAP Level□4 Soil Moisture Algorithm and Data Product. *Journal of Advances in Modeling Earth Systems*, 11. https://doi.org/10.1029/2019MS001729, 2019.

Rodell, M.; Houser, P.R.; Jambor, U.; Gottschalck, J.; Mitchell, K.; Meng, C.-J.; Arsenault, K.; Cosgrove, B.; Radakovich, J.; Bosilovich, M.; Entin, J.K.,Walker, J.P., Lohmann, D., and Toll, D. The Global Land Data Assimilation System. Bull. Am. Meteor. Soc. 85, 381–394, 2004.

Rodríguez-Fernández, N.; de Rosnay, P.; Albergel, C.; Richaume, P.; Aires, F.; Prigent, C.; Kerr, Y. SMOS Neural Network Soil Moisture Data Assimilation in a Land Surface Model and Atmospheric Impact. *Remote Sens.*, *11*, 1334. https://doi.org/10.3390/rs11111334, 2019.

Rüdiger, C.; Albergel, C.; Mahfouf, J.-F.; Calvet, J.-C.; Walker, J.P. Evaluation of Jacobians for leaf area index data assimilation with an extended Kalman filter. J. Geophys. Res. 2010.

Sawada, Y.; Koike, T. Simultaneous estimation of both hydrological and ecological parameters in an ecohydrological model by assimilating microwave signal. J. Geophys. Res. Atmos, 119, 2014.

Sawada, Y.; Koike, T.; Walker, J.P. A land data assimilation system for simultaneous simulation of soil moisture and vegetation dynamics. J. Geophys. Res. Atmos, 120, 2015.

Schellekens, J., Dutra, E., Martínez-de la Torre, A., Balsamo, G., van Dijk, A., Sperna Weiland, F., Minvielle, M., Calvet, J.-C., Decharme, B., Eisner, S., Fink, G., Flörke, M., Peßenteiner, S., van Beek, R., Polcher, J., Beck, H., Orth, R., Calton, B., Burke, S., Dorigo, W., and Weedon, G. P.: A global water resources ensemble of hydrological models: the eartH2Observe Tier-1 dataset, Earth Syst. Sci. Data, 9, 389-413, https://doi.org/10.5194/essd-9-389-2017, 2017.

Scipal, K.; Drusch, M.; Wagner, W. Assimilation of a ERS scatterometer derived soil moisture index in the ECMWF numerical weather prediction system. Adv. Water Resour., 31, 1101–1112, 2008.

Schlosser, A.; Dirmeyer, P. Potential preditability of Eurasian snow cover. Atmos. Sci. Lett., 2, 1–8, 2001.

Shamambo, D.C.; Bonan, B.; Calvet, J.-C.; Albergel, C.; Hahn, S. Interpretation of ASCAT Radar Scatterometer Observations Over Land: A Case Study Over Southwestern France. *Remote Sens.*, *11*, 2842, 2019.

Svoboda, M. Drought Monitor. Bulletin of the American Meteorological Society, pp. 1181–1190. doi:10.1175/1520-0477(2002)083<1181:TDM>2.3.CO;2., 2002

Tall, M.; Albergel, C.; Bonan, B.; Zheng, Y.; Guichard, F.; Dramé, M.S.; Gaye, A.T.; Sintondji, L.O.; Hountondji, F.C.C.; Nikiema, P.M.; Calvet, J.-C. Towards a Long-Term Reanalysis of Land Surface Variables over Western Africa: LDAS-Monde Applied over Burkina Faso from 2001 to 2018. Remote Sens., 11, 735, 2019.

Tramontana, G., Jung, M., Schwalm, C. R., Ichii, K., Camps-Valls, G., Ráduly, B., Reichstein, M., Arain, M. A., Cescatti, A., Kiely, G., Merbold, L., Serrano-Ortiz, P., Sickert, S., Wolf, S., and Papale, D.: Predicting carbon dioxide and energy fluxes across global FLUXNET sites with regression algorithms, Biogeosciences, 13, 4291–4313, https://doi.org/10.5194/bg-13-4291-2016, 2016.

Urraca, R.; Huld, T.; Gracia-Amillo, A.; Martinez-de-Pison, F.J.; Kaspar, F.; Sanz-Garcia, A. Evaluation of global horizontal irradiance estimates from ERA5 and COSMO-REA6 reanalyses using ground and satellite-based data. Sol. Energy, 164, 339–354, 2018.

Van Loon, A.F.: Hydrological drought explained. WIREs Water, 2:359–392, doi:10.1002/wat2.1085, 2015.

Voldoire, A., Decharme, B., Pianezze, J., Lebeaupin Brossier, C., Sevault, F., Seyfried, L., Garnier, V., Bielli, S., Valcke, S., Alias, A., Accensi, M., Ardhuin, F., Bouin, M.-N., Ducrocq, V., Faroux, S., Giordani, H., Léger, F., Marsaleix, P., Rainaud, R., Redelsperger, J.-L., Richard, E., and Riette, S.: SURFEX v8.0 interface with OASIS3-MCT to couple atmosphere with hydrology, ocean, waves and sea-ice models, from coastal to global scales, Geosci. Model Dev., 10, 4207-4227, https://doi.org/10.5194/gmd-10-4207-2017, 2017.

Wagner, W.; Lemoine, G.; Rott, H. A method for estimating soil moisture from ERS scatterometer and soil data. Remote Sens. Environ., 70, 191–207, 1999.

Wilhite, D.A., Drought, a global assessment. Natural Hazards and Disasters Series, vol. 1. Routledge, London, UK, 2000.

World Meteorological Organization (WMO) and Global Water Partnership (GWP). Benefits of action and costs of inaction: Drought mitigation and preparedness – a literature review (N. Gerber and A. Mirzabaev). Integrated Drought Management Programme (IDMP) Working Paper 1. WMO, Geneva, Switzerland and GWP, Stockholm, Sweden, 2017.

Xia, Y., Mitchell, K., Ek, M., Sheffield, J., Cosgrove, B., Wood, E., Luo, L., Alonge, C., Wei, H., Meng, J., Livneh, B., Lettenmaier, D., Koren, V., Duan, Q., Mo, K., Fan, Y. and Mocko, D., Continental□scale water and energy flux analysis and validation for the North American Land Data Assimilation System project phase 2 (NLDAS□2): 1. Intercomparison and application of model products, *J. Geophys. Res.*, 117, D03109, doi:10.1029/2011JD016048, 2012.

Xia, Y., Mitchell K., Ek M., Cosgrove B., Sheffield J., Luo L., Alonge C., Wei H., Meng J., Livneh B., Duan Q. and Lohmann D:,Continental□scale water and energy flux analysis and validation for North American Land Data Assimilation System project phase 2 (NLDAS□2): 2. Validation of model□simulated streamflow, *J. Geophys. Res.*, 117, D03110, doi:10.1029/2011JD016051, 2012.

Tables

Table I: Continental hot spots for droughts and heatwaves and number of monthly anomalies SSM and LAI below -1 standard deviation (stdev), above 1 stdev in 2018 with respect to the 2010-2018 period.

Region name	abbreviation	LON-W	LON-E	LAT-S	LAT-N	Number of monthly SSM anomalies below -1 (above 1) stdev	Number of monthly LAI anomalies below -1 (above 1) stdev
Western-Europe	**WEUR**	**-1**	**15**	**48**	**55**	**5(1)**	**5(0)**
Western Mediterranean	WMED	-10	15	35	45	0(7)	4(4)
Eastern Europe	EEUR	15	30	45	55	2(1)	0(2)
Balkans	BALK	15	30	40	45	3(3)	1(4)
Western Russia	WRUS	30	60	55	67	0(1)	1(3)
Lower Volga	LVOL	30	60	45	55	2(1)	2(1)
India	INDI	73	85	12	27	3(0)	2(1)
Southwestern China	SWCH	100	110	20	32	0(2)	0(6)
Northern China	NRCH	110	120	30	40	0(3)	0(4)
Murray-Darling	**MUDA**	**140**	**150**	**-37**	**-26**	**6(0)**	**7(0)**
California	CALF	-125	-115	30	42	2(0)	5(0)
Southern Plains	SPLN	-110	-90	25	37	0(3)	0(4)
Midwest	MIDW	-105	-85	37	50	1(2)	1(3)
Eastern North	ENRT	-85	-70	37	50	0(3)	0(7)
Nordeste	NDST	-44	-36	-20	-2	0(3)	1(2)
Pampas	PAMP	-64	-58	-36	-23	2(2)	2(0)
Sahel	SAHL	-18	25	13	19	2(0)	1(2)
East Africa	**EAFR**	**38**	**51**	**-4**	**12**	**2(3)**	**1(7)**
Southern Africa	SAFR	14	26	-35	-26	2(0)	2(1)

Table II: Set up of the experiments performed in this study. LDAS_ERA5 and LDAS_HRES have an analysis (assimilation of surface soil moisture, SSM, and leaf area index, LAI) and a model equivalent (open-loop, no assimilation), LDAS_fc4 and LDAS_fc8 are model runs initialized by either LDAS_HRES open-loop or analysis. N/A stands for not applicable.

<table>
<tr><th>Experiments (time period)</th><th>Model version</th><th>Atmospheric forcing</th><th>Domain & spatial resolution</th><th>DA method</th><th>Assimilated observations</th><th>Model equivalents</th><th>Control variables</th></tr>
<tr><td>LDAS_ERA5 (2010 to 2018)</td><td rowspan="4">ISBA Multi-layer soil model CO_2-responsive version (Interactive vegetation)</td><td>ERA5</td><td>Global, ~0.25 °x 0.25°</td><td rowspan="2">SEKF</td><td>SSM (ASCAT)

LAI (GEOV1)</td><td>Second layer of soil (1-4cm)

LAI</td><td>Layers of soil 2 to 8 (1-100cm)

LAI</td></tr>
<tr><td>LDAS_HRES (04/2016 to 12/2018)</td><td rowspan="3">IFS-HRES</td><td rowspan="3">North Western Europe (WEUR) and Murray-Darling River basin (MUDA) (see spatial extend in Table I) ~0.10° x 0.10°</td></tr>
<tr><td>LDAS_fc4 (2017 to 2018)</td><td rowspan="2">N/A</td><td rowspan="2">N/A</td><td rowspan="2">N/A</td><td rowspan="2">N/A</td></tr>
<tr><td>LDAS_fc8 (2017 to 2018)</td></tr>
</table>

Table III: Evaluation datasets and associated metrics used in this study.

Datasets used for the evaluation	**Source**	**Metrics associated**	**Independent source of evaluation**
In situ measurements of soil moisture (ISMN Dorigo et al., 2011, 2015)	https:// ismn.geo.tuwien.ac.at/ en/	R for both absolute and anomaly time-series, unbiased RMSD and bias, NIC on R values	Yes
In situ measurements of river discharge	See Table S1	Nash Efficiency (NSE), Normalized Information Contribution (NIC) based on NSE,	Yes
In situ measurements of evapotranspiration (FLUXNET-2015)	http:// fluxnet.fluxdata.org/ data/fluxnet2015-dataset/	R, unbiased RMSD, Bias, NIC on R values	Yes
Satellite derived surface soil wetness index (ASCAT, Wagner et al., 1999, Bartalis et al., 2007)	http:// land.copernicus.eu/ global/	R, RMSD and N_{RMSD}	No (assimilated dataset)
Satellite derived Leaf Area Index (GEOV1, Baret et al., 2013)	http:// land.copernicus.eu/ global/	R, RMSD and N_{RMSD}	No (assimilated dataset)
Satellite-driven model estimates of land evapotranspiration (GLEAM, Martens et al., 2017)	http://www.gleam.eu	R, RMSD and N_{RMSD}	Yes
Upscaled estimates of Gross Primary Production (GPP, Jung et al., 2017)	https://www.bgc-jenna.mpg.de/geodb/ projects/Home.php	R, RMSD and N_{RMSD}	Yes
Solar Induced Fluorescence (SIF) from GOME-2 (Munro et al., 2006, Joiner et al., 2016)	See references	R	Yes
Interactive Multi-sensor Snow and Ice Mapping System (or IMS) snow cover	https:// www.natice.noaa.gov/ ims/	Differences	Yes

Figures

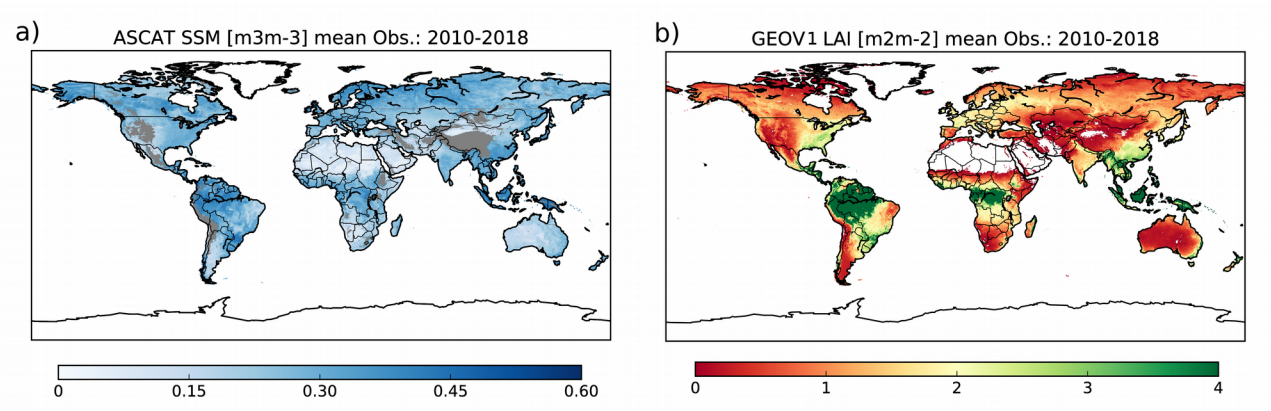

Figure 1: (a) Surface soil moisture (SSM) from the Copernicus Global Land Service (CGLS) for pixels with less than 15% of urban areas and with an elevation of less than 1500 m above sea level, (b) GEOV1 leaf area index (LAI) from CGLS, for pixels covered by more than 90 % of vegetation, averaged over 2010 to 2018. SSM is obtained after rescaling the ASCAT Soil Wetness Index (SWI) to the model climatology, grey areas on (a) represent filtered out data (see Section 2.3).

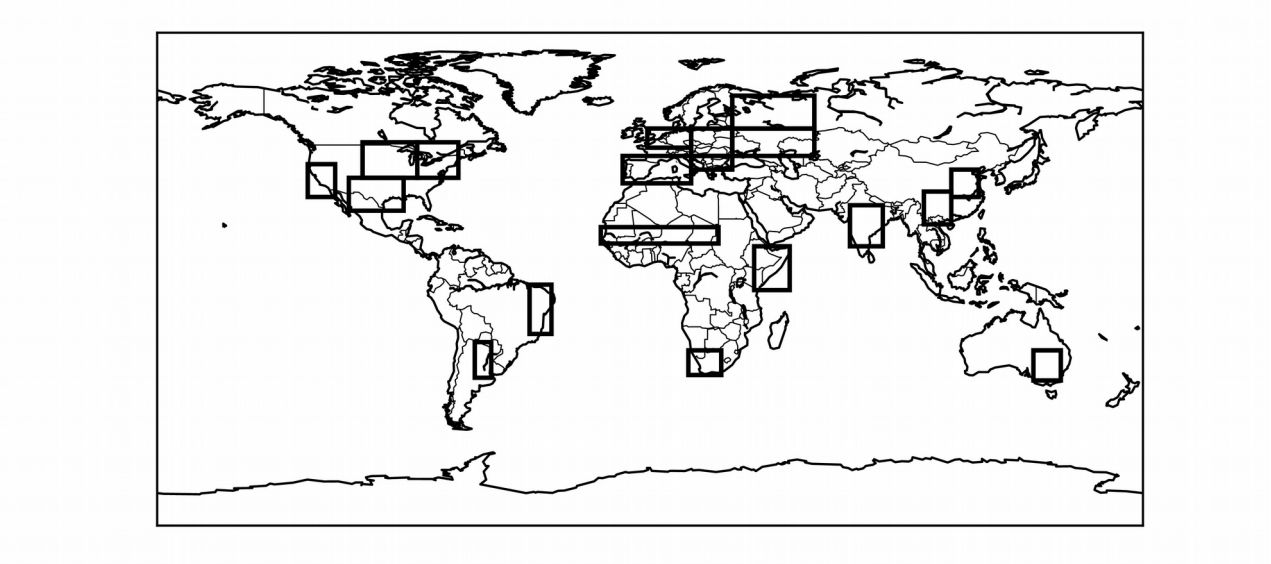

Figure 2: Selection of 19 regions across the globe known for being potential hot spots for droughts and heatwaves. The regions are defined in Table I.

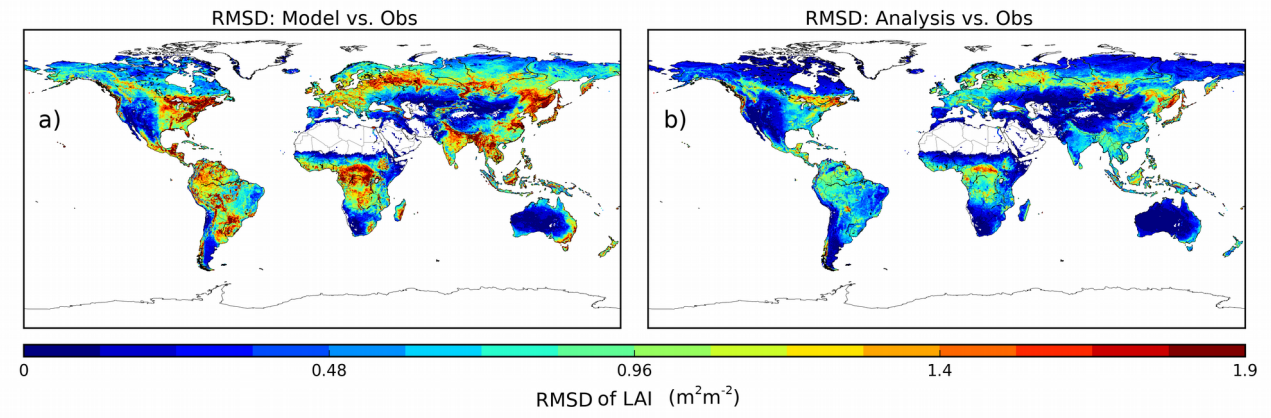

Figure 3: RMSD values between observed Leaf Area Index (LAI) and LDAS_ERA5 (a) before assimilation and (b) after assimilation of surface soil moisture (SSM) and LAI.

1150

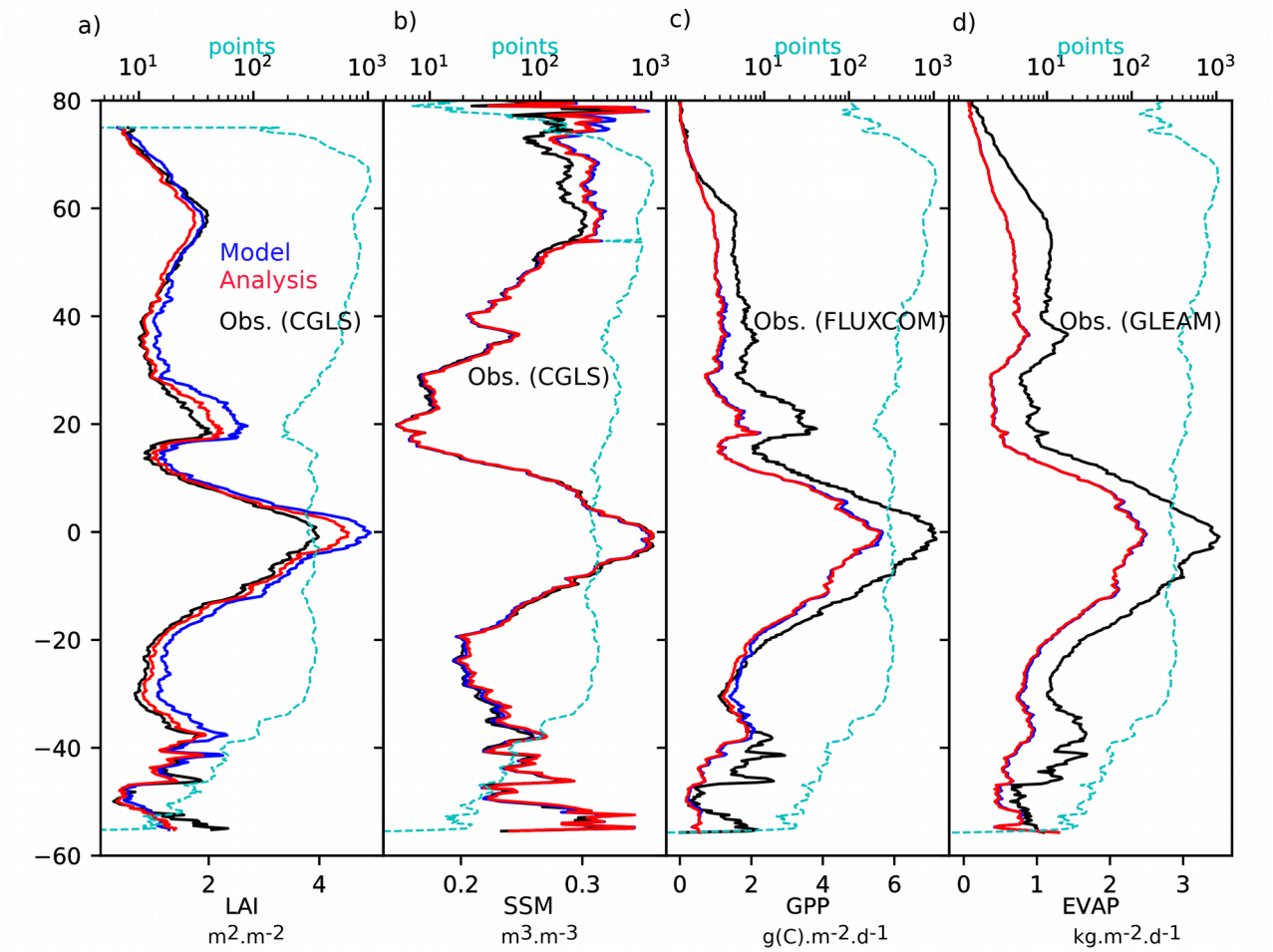

Figure 4: Latitudinal plots of (a) Leaf Area Index (LAI), (b) Surface Soil Moisture (SSM), (c) Gross Primary Production (GPP) and (d) Evapotranspiration (EVAP) for LDAS_ERA5 before assimilation (Model, blue solid line) and after assimilation (Analysis, red solid line) as well as observations (black solid line). Cyan dashed line represents the number of points considered per latitudinal stripes of 0.25°.

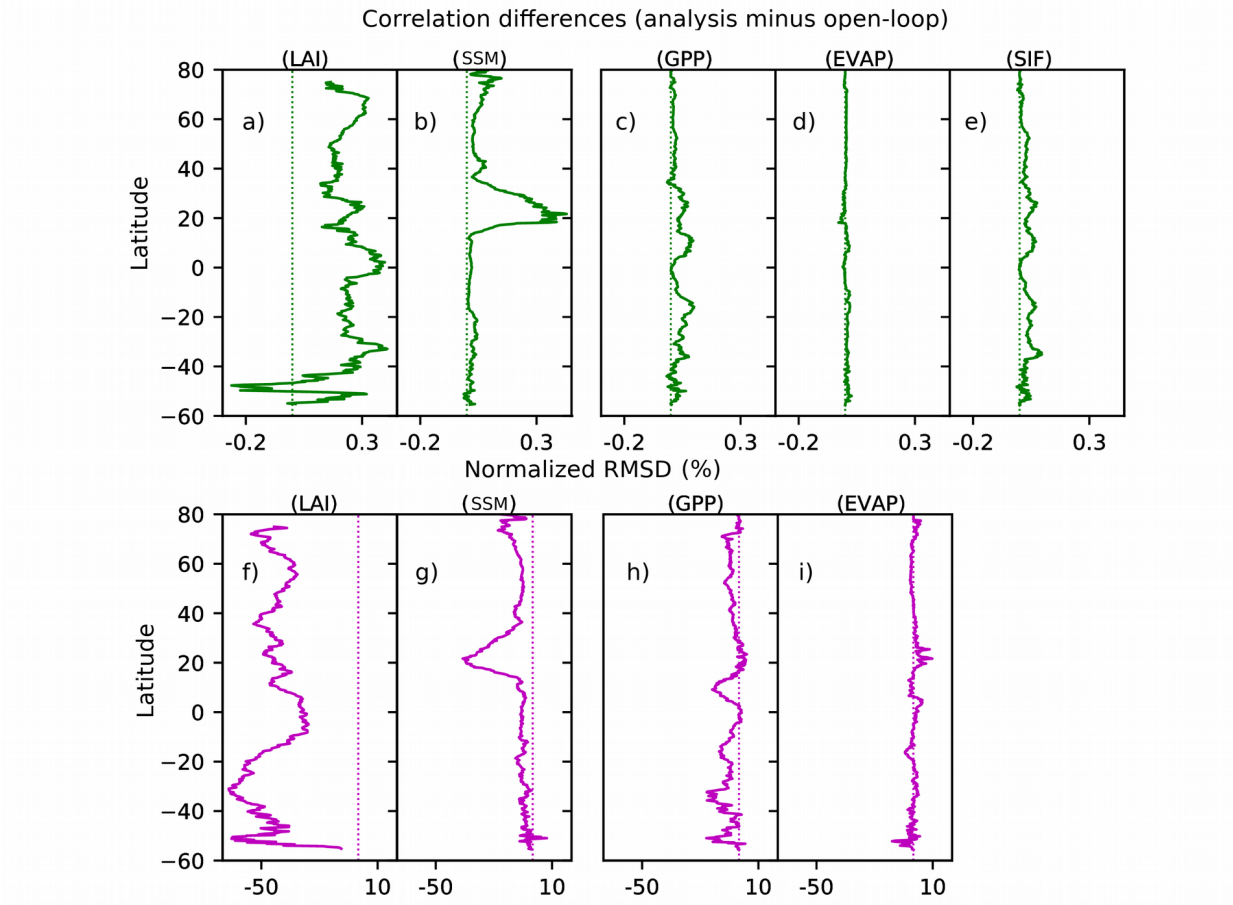

Figure 5: Latitudinal plots of score differences (analysis minus open-loop) for correlations (a-e) and normalized RMSD (f-i) for LAI (a,f), SSM (b,g), GPP (c,h), EVAP (d,i) and SIF (e, correlations only). Scores are computed based on monthly average over 2010-2018 for LAI and SSM, 2010-2013 for GPP, 2010-2016 for EVAP and 2010-2015 for SIF. Dashed lines represent the zero lines (equal scores for open-loop and analysis).

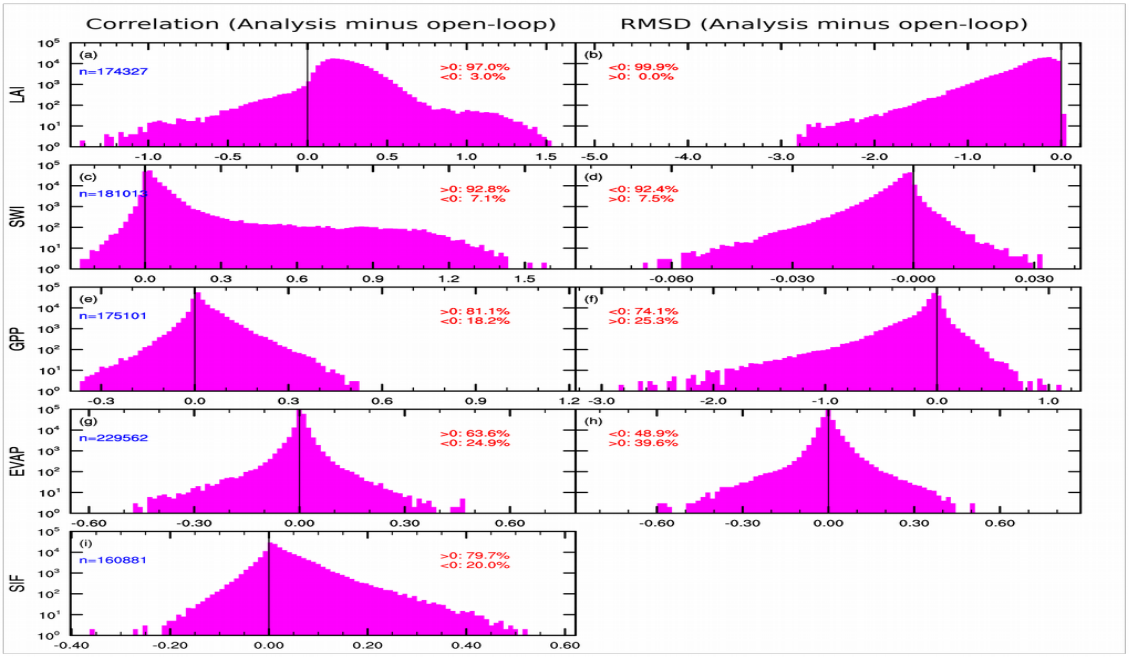

Figure 6: Histograms of score differences (correlation and RMSD, analysis minus open-loop) for a),b) LAI, c),d) SSM, e),f) GPP, g),h) EVAP and i) SIF. For SIF only differences in correlation are represented. Number of available data (in blue) as well as the percentage of positive and negative values (in red) are reported. Note that for sake of clarity, the y-axis is logarithmic.

1165

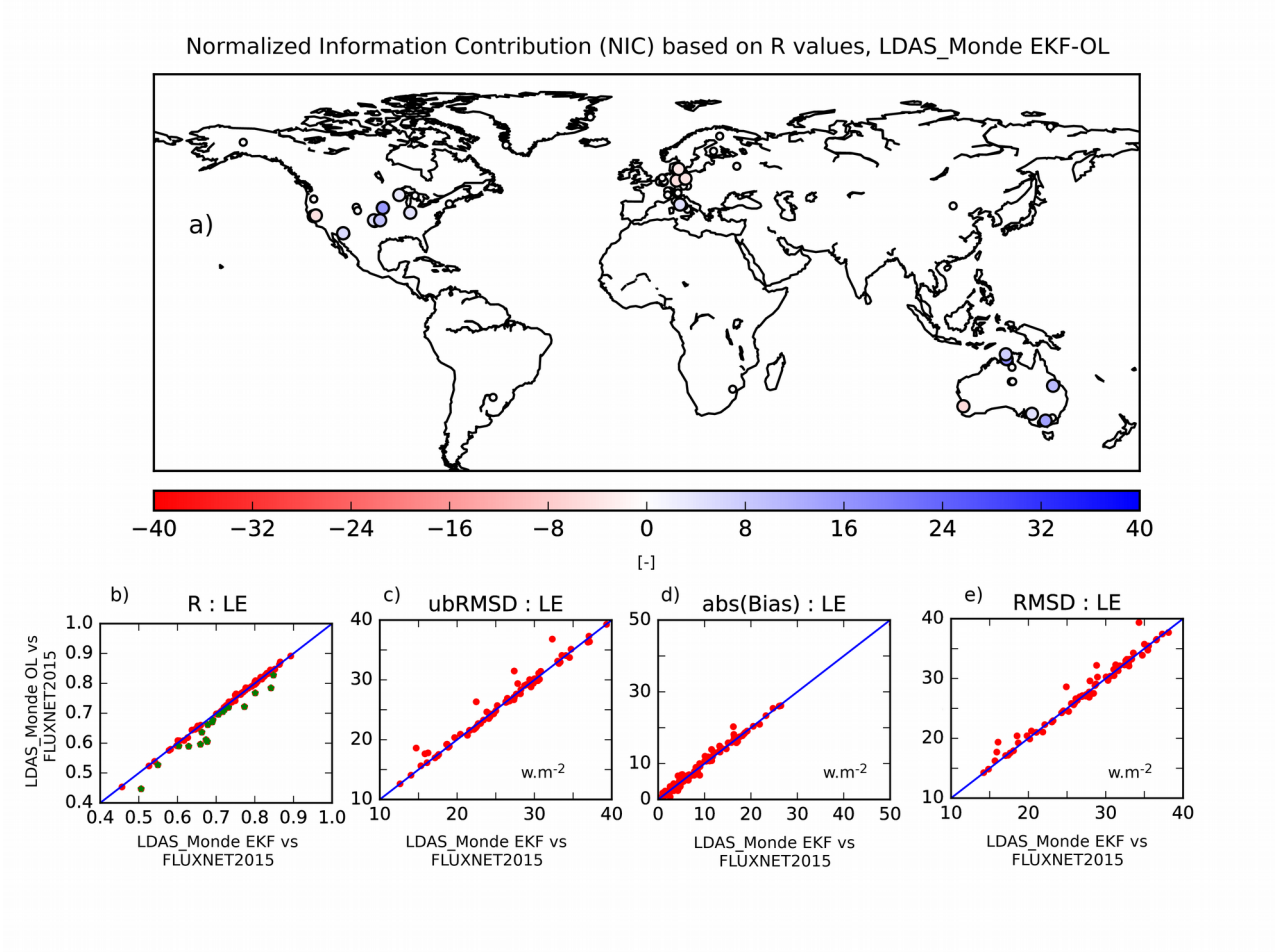

Figure 7:(a) Map of Normalized Information Contribution (NIC, Eq. 2) applied on correlation values between evapotranspiration from LDAS_ERA5 analysis (open-loop) and observations from the FLUXNET 2015 synthesis data set. NIC scores are classified into 2 categories (i) negative impact from the analysis with respect to the model with values smaller than -3 % (red circles, 5 stations), (ii) positive impact from the analysis with respect to the model with values greater than +3 % (blue circles, 20 stations). Stations presenting a neutral impact with values between -3 % and +3 % (60 stations) are reported as small dots. Note that at this scale some stations are overlapping. (b), (c), (d) and (e) scatter-plots of R, ubRMSD, absolute bias and RMSD between LDAS_ERA5 open-loop and the 85 stations from the FLUXNET 2015 (y-axis) and LDAS_ERA5 analysis and the same pool of stations (x-axis). The set of 20 stations for which the analysis has a positive impact in R values at NIC_R greater than +3 are reported on a) in green.

1170

1175

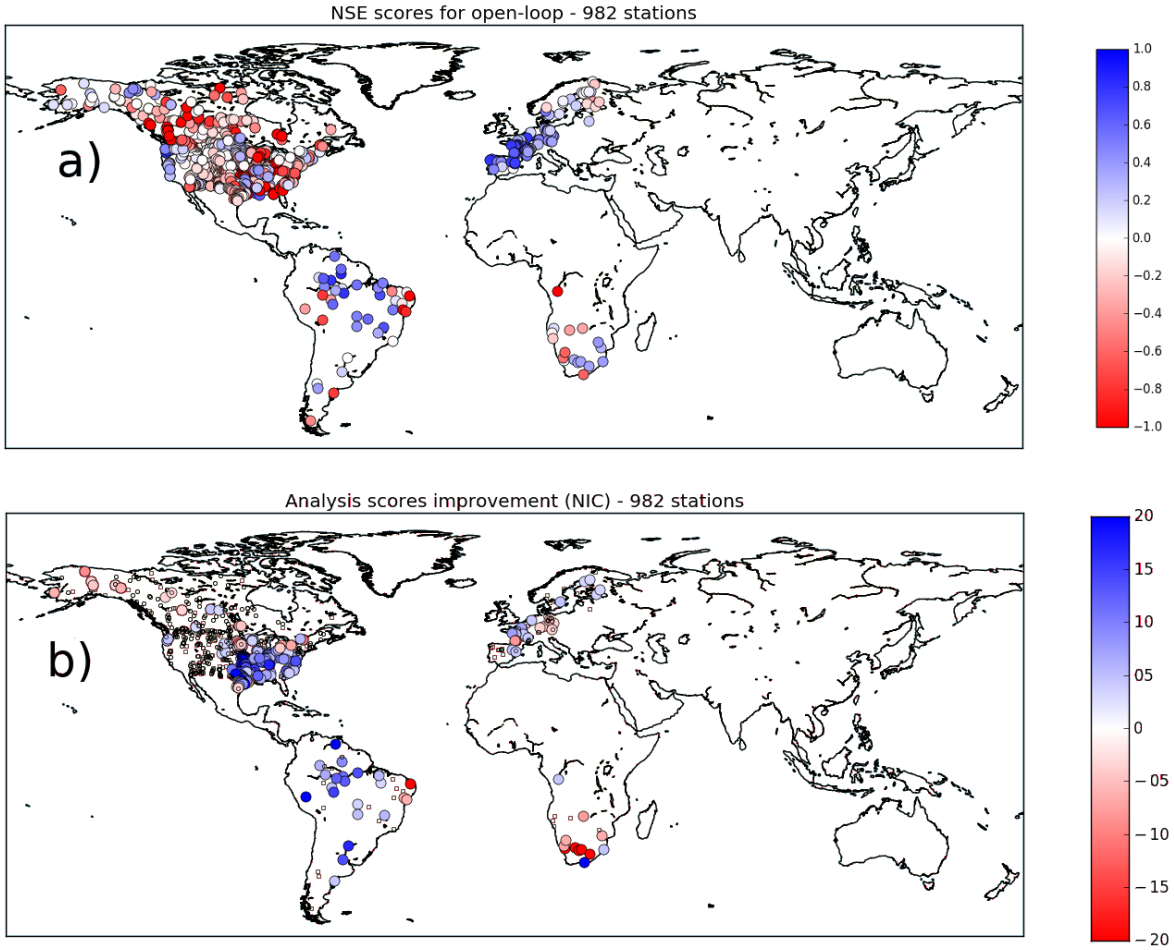

Figure 8:(a) Global map of Nash-Sutcliff Efficiency score (NSE) between river discharge from LDAS_ERA5 open-loop and in situ measurements from the networks presented in Table S1 over 2010-2016. (b) Normalized Information Contribution scores (NIC, Eq.2) based on NSE scores on river discharge. Small dots represent stations for which NIC are between [-3%, +3%] (i.e. neutral impact from LDAS_ERA5 analysis), NIC values greater than +3% (blue large circles) suggest an improvement from LDAS_ERA5 analysis over LDAS_ERA5 open-loop while values smaller than -3% (large red circles) suggest a degradation. Only stations where more than 4-year of data are available and with a drainage area greater than 10000km^2 are considered. Stations with NSE values smaller than -2 are discarded, also, leading to a subset of 982 stations available.

1180

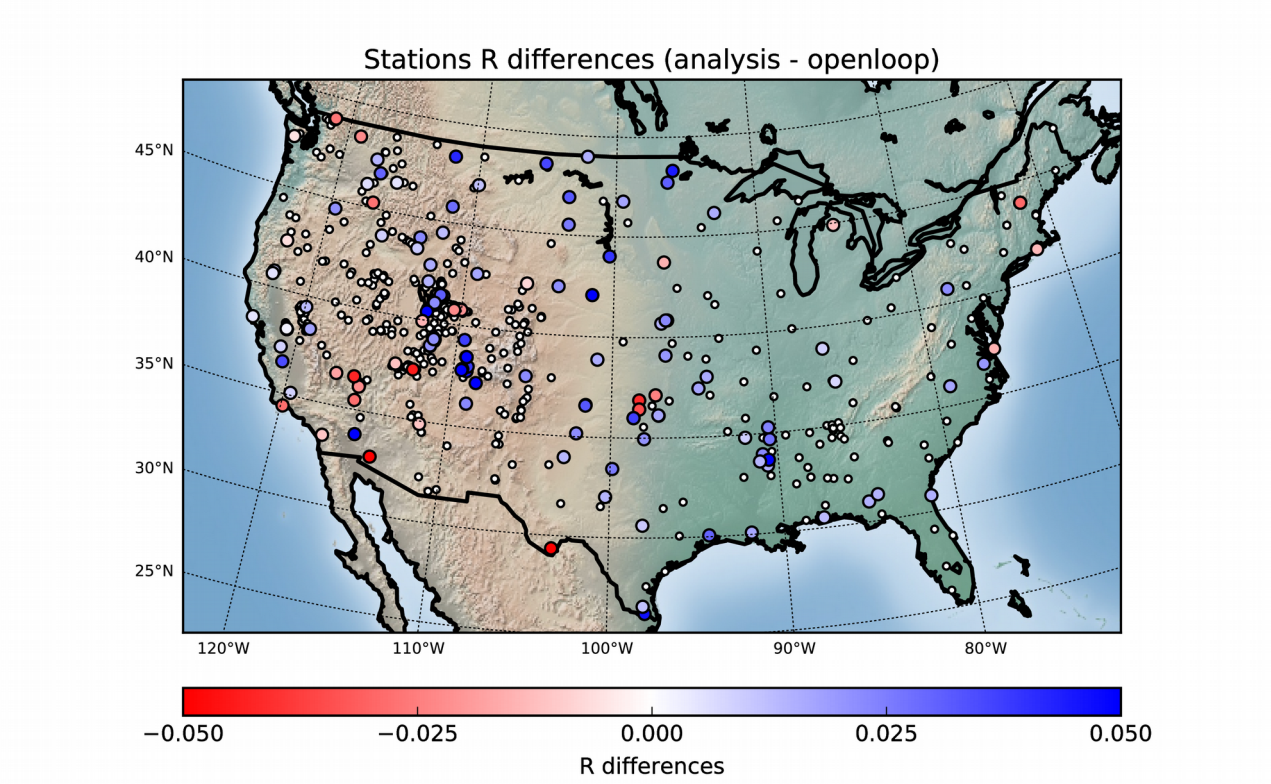

Figure 9: Map of correlations (R) differences (analysis minus open-loop) for stations measuring soil moisture at 5 cm depth and being available over North America. Small dots represent stations where R differences are not significant (i.e. 95% confidence intervals are overlapping), large circles where differences are significant.

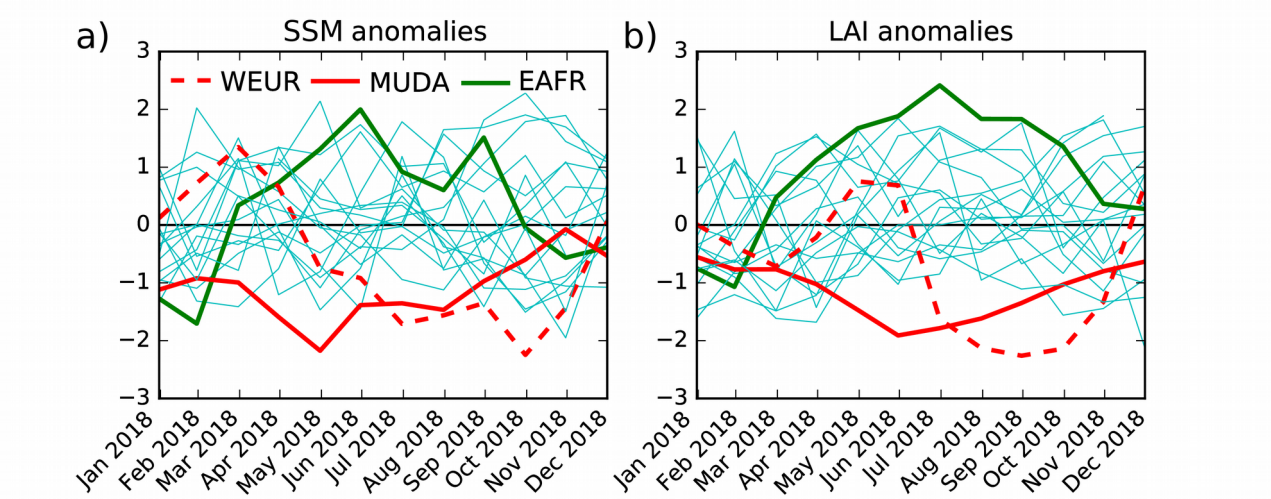

Figure 10: 2018 monthly anomalies scaled by standard deviation of analysed (a)SSM and (b)LAI, with respect to 2010-2018, for the 19 regions presented in Table 1 and Figure 2. Solid red line, dashed red line and solid green line represent regions MUDA, WEUR and EAFR. Solid cyan line represent all other boxes (see Table 1 and Figure 2).

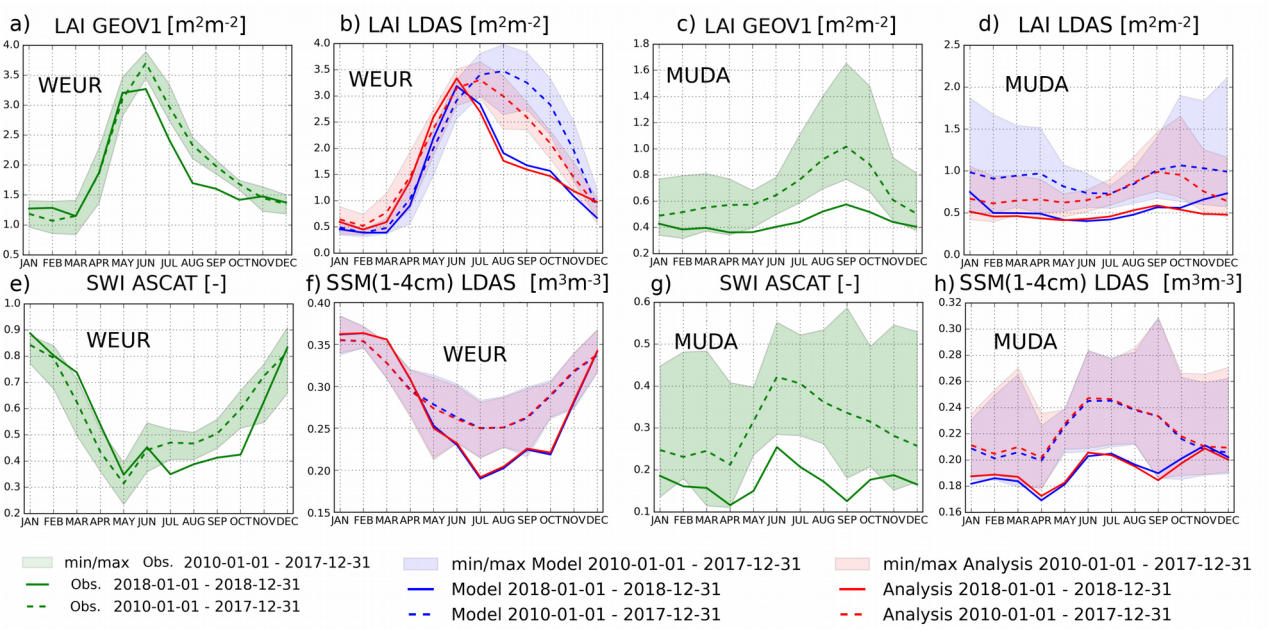

Figure 11: Upper panels represent seasonal cycles of a) observed GEOV1 LAI from CGLS, b) LAI from the open-loop (in blue) and the analysis (in red) for the WEUR area (see Table I for geographical extent). c) and d) panels are similar to a) and b) for the MUDA area . Lower panels represents seasonal cycles of e) ASCAT SWI from CGLS, f) SSM from the open-loop (in blue) and the analysis (in red) for the WEUR area. Panels g) and h) are similar to e) and f) for the MUDA area. For each panels dashed line represents the averaged over 2010-2017 along with the minimum and maximum values, the solid lines are for the year 2018.

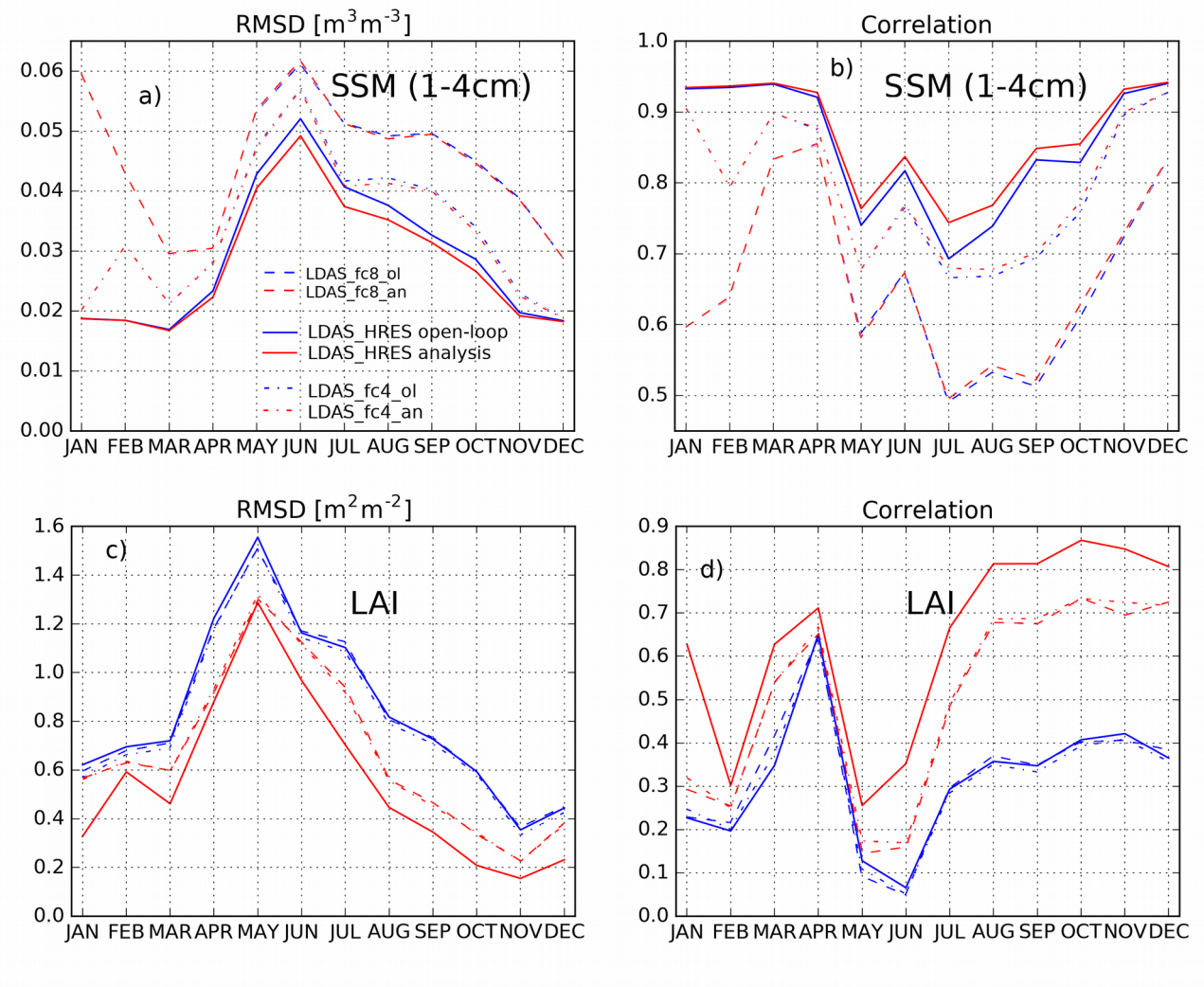

Figure 12: Upper panel, seasonal (a) RMSD and (b) correlation values between soil moisture from the second layer of soil (1–4 cm) from the model forced by HRES (LDAS_HRES, open-loop in blue solid line, analysis in red solid line) and ASCAT SSM estimates over 2017-2018 over the WEUR area. Scores between SSM from the second layer of soil of LDAS_HRES, 4-day (dashed/dotted blue – when initialised by the open-loop- and red – when initialised by the analysis- lines) and 8-day (dashed blue and red lines) forecasts and ASCAT SSM estimates are also reported. Lower panel (c) and (d) , same as upper panel between modeled/analyzed Leaf Area index (LAI) and GEOV1 LAI estimates .

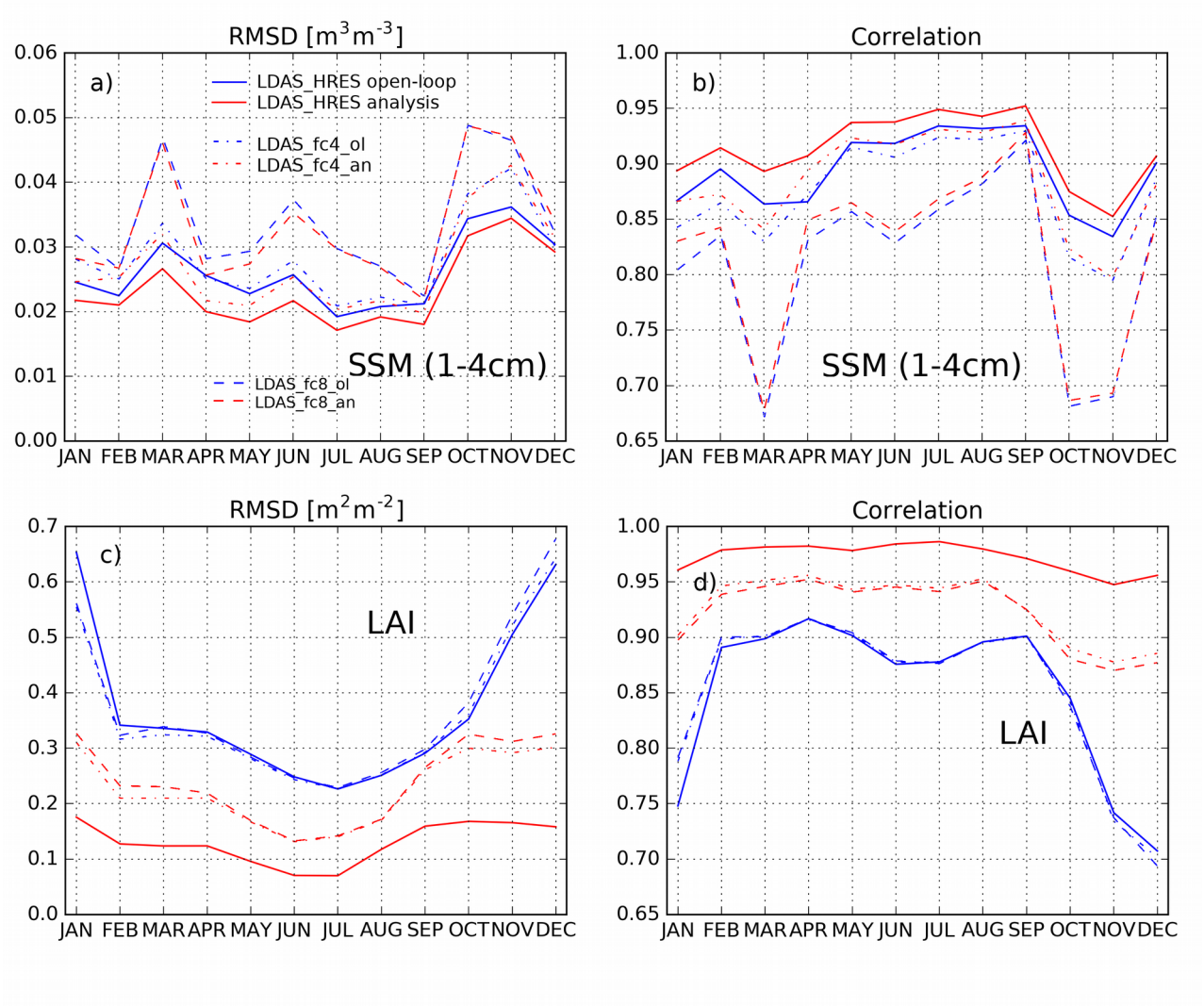

Figure 13: Same as Figure 12 for the Murray-Darling river (MUDA) area in South Eastern Australia.

1205

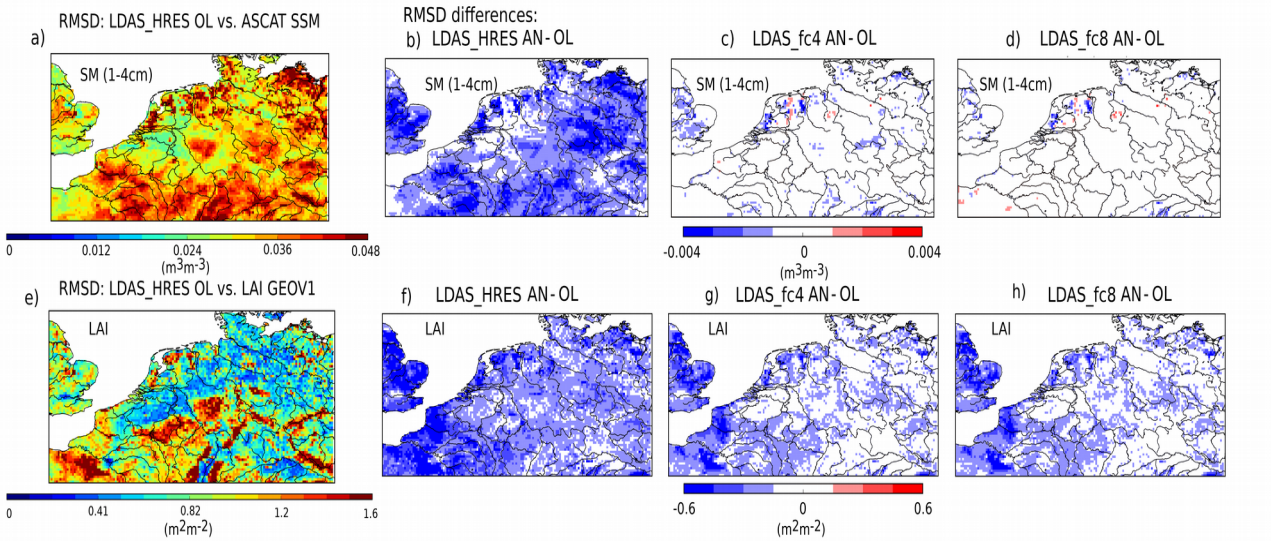

Figure 14: Top row, (a) RMSD values between LDAS_HRES open-loop and ASCAT SSM estimates over 2017-2018 for the WEUR domain, (b) RMSD differences between LDAS_HRES analysis (open-loop) and ASCAT SSM. (c), (d) and (e) Same as (b) between LDAS_fc4 initialised by the analysis (open-loop) and LDAS_fc8. Bottom row, same as top row for LAI from the different experiments and LAI GEOV1.

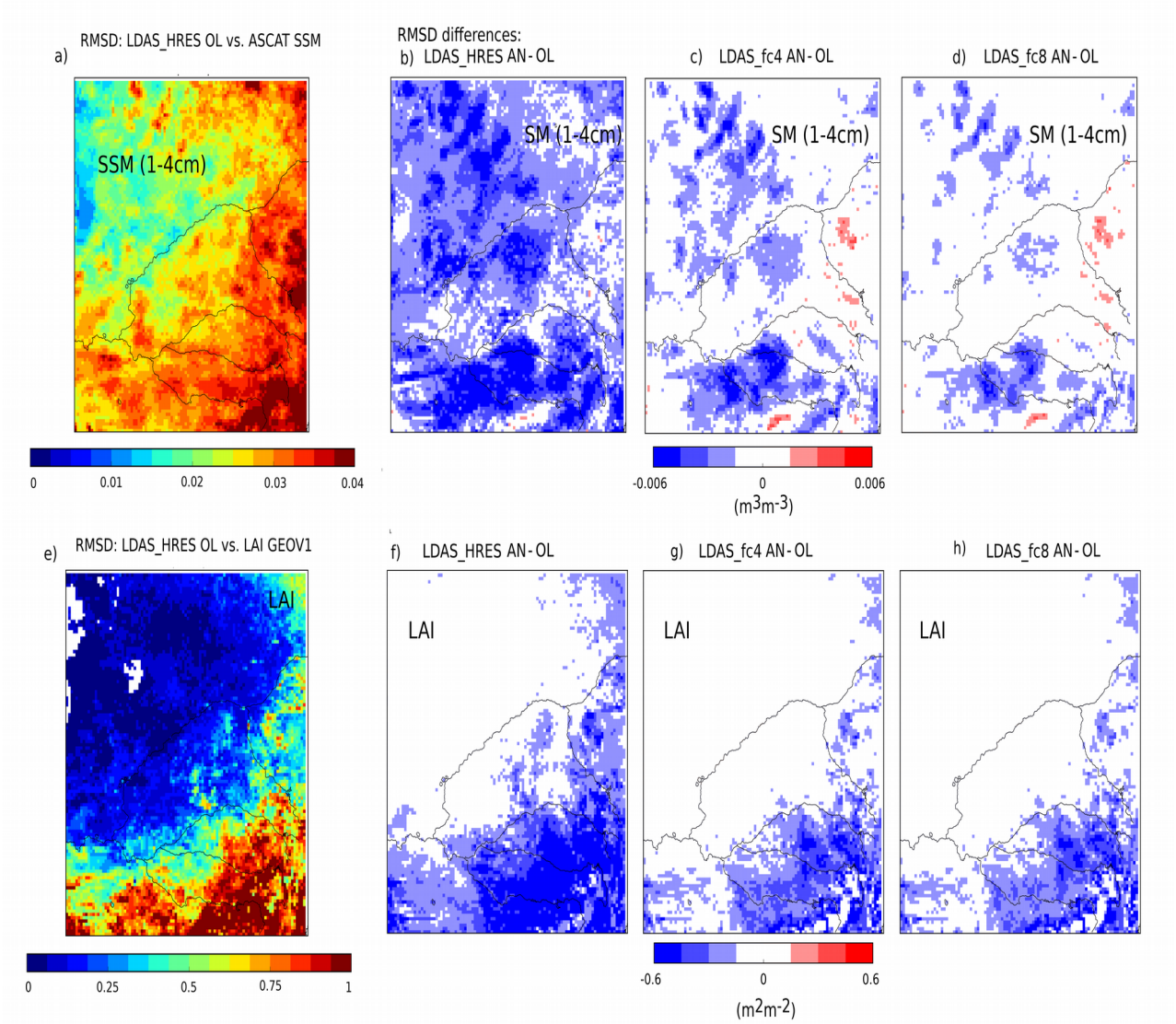

Figure 15: Same as Figure 14 or the Murray-Darling river (MUDA) area in South Eastern Australia.

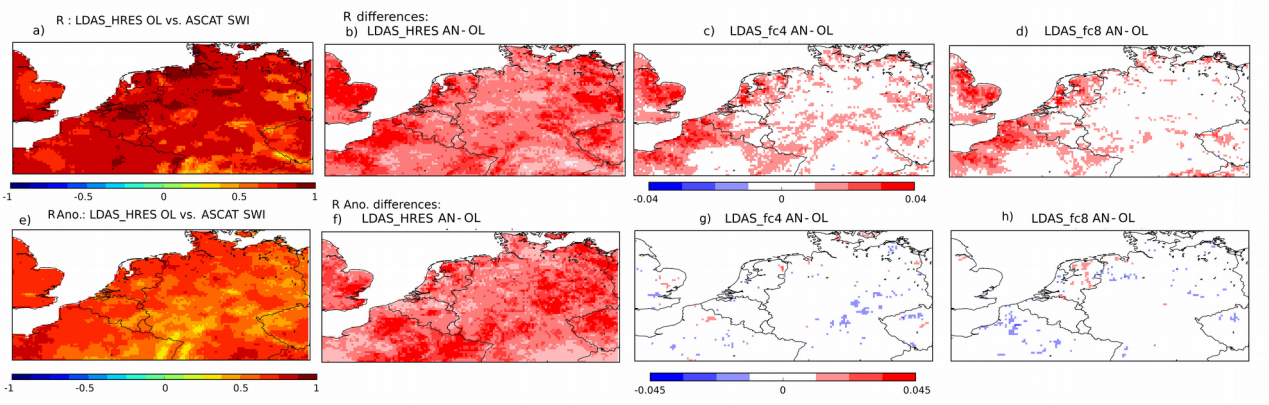

Figure 16: Top row, (a) R values between LDAS_HRES open-loop and ASCAT SWI estimates over 2017-2018 for the WEUR domain, (b) R differences between LDAS_HRES analysis (open-loop) and ASCAT SWI. (c) and (d) same as (b) between LDAS_fc4 initialised by the analysis (open-loop) and LDAS_fc8. Bottom row, same as top row for R values based on anomaly time-series.

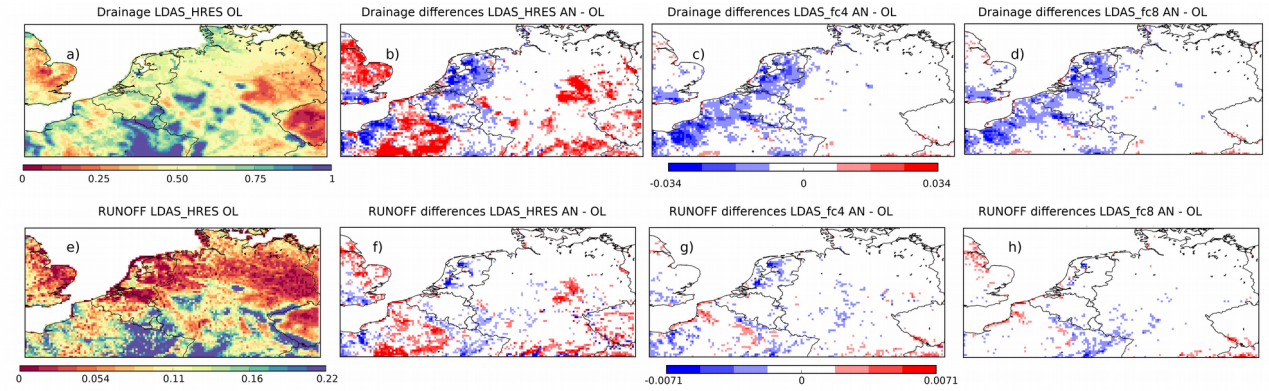

Figure 17: Top row, (a) drainage values for LDAS_HRES open-loop over 2017-2018 for the WEUR domain, (b) drainage differences between LDAS_HRES analysis and open-loop. (c), (d), same as (b) between LDAS_fc4 initialised by the analysis and LDAS_fc4 initialised by the open-loop, between LDAS_fc8 initialised by the analysis and LDAS_fc8 initialised by the open-loop. Bottom row, same as top row for runoff. Units are $kg.m^{-2}.day^{-1}$